

Northern Hemisphere Storminess in the Norwegian Earth System Model (NorESM1-M)

E.M. Knudsen^{1,2} and J.E. Walsh³

¹Geophysical Institute, University of Bergen, P.O. Box 7803, 5020 Bergen, Norway

²Bjerknes Centre for Climate Research, Bergen, Norway

³International Arctic Research Center, University of Alaska Fairbanks, 930 Koyukuk Drive, Fairbanks, Alaska 99775–7340, USA

Correspondence to: E.M. Knudsen (erlend.knudsen@gfi.uib.no)

Abstract. Metrics of storm activity in Northern Hemisphere high- and midlatitudes are evaluated from historical output and future projections by the Norwegian Earth System Model (NorESM1-M) coupled global climate model. The European Re-Analysis Interim (ERA-Interim) and the Community Climate System Model (CCSM4), a global climate model of the same vintage as NorESM1-M, provide benchmarks for comparison. The focus is on the autumn and early winter (September through December) — the period when the ongoing and projected Arctic sea ice retreat is greatest. Storm tracks derived from a vorticity-based algorithm for storm identification are reproduced well by NorESM1-M, although the tracks are somewhat better resolved in the higher-resolution ERA-Interim and CCSM4. The tracks show indications of shifting polewards in the future as climate changes under the Representative Concentration Pathway (RCP) forcing scenarios. Cyclones are projected to become generally more intense in the high-latitudes, especially over the Alaskan region, although in some other areas the intensity is projected to decrease. While projected changes in track density are less coherent, there is a general tendency towards less frequent storms in midlatitudes and more frequent storms in high-latitudes, especially the Baffin Bay/Davis Strait region in September. Autumn precipitation is projected to increase significantly across the entire high-latitudes. Together with the projected increases in storm intensity and sea level and the loss of sea ice, this increase in precipitation implies a greater vulnerability to coastal flooding and erosion, especially in the Alaskan region. The projected changes in storm intensity and precipitation (as well as sea ice and sea level pressure) scale generally linearly with the RCP value of the forcing and with time through the 21st century.

20 1 Introduction

The climate of the recent decades has undergone a warming that has been amplified in the Arctic. This polar amplification, due in part to the reduction of sea ice and snow cover, has resulted in an Arctic warming that is twice as large as the global mean (e.g., Bekryaev et al., 2010; AMAP, 2011). The warming of the Arctic has contributed to, and been increased by, the loss of sea ice
25 (Stocker et al., 2013). Other important factors contributing to polar amplification appear to be the lapse rate feedback, the increase in atmospheric humidity and the fact that longwave radiation to space increases less under global warming in the cold polar regions than in the tropics (the so-called Planck Effect; Pithan and Mauritsen, 2014). Impacts of sea ice loss and Arctic warming on the atmospheric circulation in the high- and midlatitudes have been suggested by the studies of Overland
30 and Wang (2010), Francis and Vavrus (2012) and Cohen et al. (2012), although the robustness of the midlatitude impacts has been questioned (Barnes, 2013; Barnes et al., 2014; Screen and Simmonds, 2013). Whether or not a large-scale signal of Arctic warming and sea ice loss has yet emerged from the noise of internal variability, climate models project continued Arctic warming and sea ice loss through the 21st century, increasing the likelihood of associated changes in the large-scale
35 circulation.

Much of the effort to diagnose and project Arctic change has focused on temperature, sea ice and precipitation. However, climate-driven changes in storms are arguably more important considerations for Arctic residents, as well as for the heat and moisture budgets of the atmosphere. The impacts of storms are magnified by the loss of sea ice, which increases wave activity, coastal flood-
40 ing and erosion and also increases the risks of vessel icing in waters newly accessible for marine transport and for other offshore activities (AMAP, 2005).

Analyses of observational data have produced mixed results on trends of high-latitude storminess. In earlier studies, Zhang et al. (2004) found an increase of Arctic cyclone activity, while McCabe et al. (2001) reported northward shifts of storm tracks over the Northern Hemisphere (NH) over the
45 last several decades of the 20th century. Wang et al. (2006) detected a northward shift of cyclone activity, primarily during winter, over Canada during 1953–2002, and this meridional shift was confirmed more generally in a more recent study by the same group (Wang et al., 2013). The recent U.S. National Climate Assessment (Melillo et al., 2014) points to a poleward shift of storm tracks over the United States during recent decades. However, Mesquita et al. (2010) found that temporal trends of
50 cyclones in the North Pacific Ocean have generally been weak over the 60-year period ending 2008. The U.S. Global Change Research Program (Karl et al., 2009) points to an increase of storminess on the northern Alaskan coast and to associated risks of flooding and coastal erosion along with expected sea level rise. Since any increases of coastal flooding and erosion are also related to retreating sea ice, storms in coastal areas of the Arctic can pose increasing risks regardless of whether storm
55 activity is changing.

Previous work addressing cyclone-sea-ice linkages has shown increasing cyclone strength occurring with decreasing September sea ice edge, though no relationship with cyclone counts was found (Simmonds and Keay, 2009). Increasing amounts of open water in the Arctic enhance exchanges of heat, moisture, and momentum between the surface and atmosphere as a cyclone passes. Depending on the track of a cyclone, these additional fluxes can impact cyclone development. Two studies, one an evaluation of midlatitude marine cyclones (Kuo et al., 1991) and the other a case study of summer Arctic cyclones (Lynch et al., 2003), found surface energy flux input to be most important in the initial formation stages of the cyclone. Inputs in the later stages of the cyclone life cycle showed little impact. Furthermore, two case studies of Arctic cyclones found that increased surface energy fluxes in the later stages of the cyclone were not enough to overcome the large-scale dynamics (Long and Perrie, 2012; Simmonds and Rudeva, 2012). However, the former study indicated increased maximum wind speeds as the cyclone studied moved over open water, primarily through enhanced momentum exchange between the surface and atmosphere compared to what would occur over sea ice. These results indicate that the cyclone track is rather important as to whether or not changing surface conditions will significantly impact cyclone development.

Global climate models are arguably the best tools for identifying externally forced signals (greenhouse gases and aerosols) in storm activity. In this study, we seek to validate the storm track components of two state-of-the-art global climate models over midlatitudes and high-latitudes of the NH. This is done through a comparison to a reanalysis data set. The models are the Norwegian Earth System Model version 1 with intermediate resolution (NorESM1-M) and the Community Climate System Model version 4 (CCSM4). The simulations examined here were performed as part of the Coupled Model Intercomparison Project phase 5 (CMIP5; Taylor et al., 2012). After assessing the models' ability to capture the primary cyclone characteristics over a recent historical period, we compare the future changes of high- and midlatitude storms through the late 21st century. This evaluation is both a comparison between the time periods for each model and a model intercomparison on diverging changes towards the late 21st century. The primary metrics of storm activity here are frequency (track density) and intensity (mean intensity).

The impacts of a warming climate on high-latitude storms are difficult to anticipate. Both models undergo Arctic-amplified warming at low levels associated with significant loss of sea ice cover in the 21st century simulations examined here. On the one hand, the increased surface fluxes of heat and moisture might be expected to fuel more and stronger storms. On the other hand, the polar amplification decreases the low-level meridional temperature gradients, reducing the potential for storm activity. Nevertheless, because upper-level temperatures show greater increases in the tropics than in the Polar Regions, upper-level meridional temperature gradients actually increase (Harvey et al., 2015). Hence, the net effect on baroclinicity cannot be simply related to baroclinic disturbances such as extratropical cyclones (Ulbrich et al., 2009). Moreover, the Arctic amplification affects the variability of the jet stream, which is directly linked to the vertically integrated meridional temperature

gradient via the thermal wind equation. Barnes and Screen (2015) provide a diagnostic assessment of these connections. Here, the model set-up implies that impacts of Arctic warming, sea ice loss
95 and changes in surface fluxes and temperature gradients are implicit in our results.

The paper is organized as follows: Section 2 describes the models, reanalysis and methods used in this study. Section 3 presents the results of the comparison with the historical reanalysis and an overview of the primary changes in the storm metrics over the 21st century, followed by a discussion of the changes in the context of earlier studies and possible future implications. Finally, Sect. 4
100 concludes with a summary of the results, uncertainties and ideas for future work.

2 Data sets and methods

The present study uses two global climate models, NorESM1-M and CCSM4, both of which are coupled atmosphere-ocean-land-sea ice models. In keeping with the theme of this special issue, we emphasize NorESM1-M and its simulations. The output of CCSM4, which has somewhat finer
105 resolution, is also examined since its storm simulations can serve as a benchmark for NorESM1-M. The following is a more complete description of NorESM1-M.

NorESM1-M is a global, coupled model system for the physical climate system. It is a joint model effort of eight Norwegian research institutions, building on and replacing the Bergen Climate Model (BCM; Furevik et al., 2003) as the Norwegian CMIP model in the Intergovernmental Panel
110 on Climate Change (IPCC) assessment reports.

NorESM1-M is described in more detail in Bentsen et al. (2013) and Iversen et al. (2013). It is based on CCSM4 and the Community Earth System Model (CESM) projects at the National Center for Atmospheric Research (NCAR) on behalf of the University Corporation for Atmospheric Research (UCAR; Gent et al., 2011). However, NorESM1-M differs from CCSM4 in the following
115 components: its own developed code for chemistry-aerosol-cloud-radiation interactions in the atmospheric module (CAM4-Oslo; Kirkevåg et al., 2013); an isopycnic coordinate ocean general circulation model developed in Bergen (e.g., Drange et al., 2005) and originating from the Miami Isopycnic Coordinate Ocean Model (MICOM; Bleck et al., 1992); and a biogeochemical ocean module from the HAMBURG Ocean Carbon Cycle (HAMOCC) model developed at the Max Planck Institute for
120 Meteorology (MPI) in Hamburg (Maier-Reimer, 1993; Maier-Reimer et al., 2005) and adapted to the isopycnic ocean model framework (Tjiputra et al., 2010).

In this study, the first version of NorESM with intermediate resolution is presented. Known formally as NorESM1-M, the model has a horizontal resolution of approximately 2° for atmosphere and land components and 1° for ocean and ice components. Its vertical resolution consists of 26
125 levels of hybrid sigma-pressure coordinates with a model top of 2.9 hPa. For brevity, the model is denoted as NorESM throughout this paper.

CCSM4 has twice the horizontal resolution of NorESM, with $1.25^\circ \times 0.90^\circ$ horizontal resolution and 26 vertical layers. It is developed at UCAR and maintained by NCAR. Described in more detail by Gent et al. (2011), CCSM4 consists of five geophysical models: atmosphere (Community Atmosphere Model; CAM4), land (Community Land Model; CLM4), ocean (Parallel Ocean Program; POP2), land ice (GLC), sea ice (Los Alamos Sea Ice Model/Community Ice CodE; CICE4), and a coupler (CPL7) that coordinates the models and sends information between them. de Boer et al. (2012) and other accompanying papers in the same CCSM4 special issue of the *Journal of Climate* assess the performance of CCSM4. For the remainder of this paper, CCSM4 will be denoted as CCSM for brevity. Apart from differences in the realizations, systematic divergence between the two models highlights the role of the ocean, sea ice and atmospheric chemistry in the climate system with other model components being similar.

Only one ensemble member of each model (NorESM: r1i1p1, CCSM: r6i1p1) is examined in the present study because only these ensemble members meet our required criteria for temporal resolution (6-hourly output is needed for cyclone tracking) and choice of scenarios. Because of this data limitation there is only a thin base for overall evaluation of storminess in CMIP5 models. However, we use multidecadal time slices in order to minimize the effects of internal variations, which account for differences across ensemble members of simulations by any one model. Moreover, Walsh et al. (2008) found that the spread within ensemble members of a single model is much smaller than inter-model spread when Arctic-averaged temperatures are compared.

The analysis involves three time periods of 27 years each and two Representative Concentration Pathways (RCPs). For the historical time period, 1979–2005, NorESM and CCSM are compared to the European Re-Analysis Interim (ERA-Interim; here abbreviated ERA-I) data set (Dee et al., 2011). ERA-I is a high-resolution reanalysis set in space and time, and is well suited for the northern regions (Jakobson et al., 2012; Chung et al., 2013), especially for storm tracking (Hodges et al., 2011; Zappa et al., 2013a).

For the historical time period, the three data sets are interpolated to a $1^\circ \times 1^\circ$ regular latitude-longitude grid for comparison. NorESM and CCSM historical means are also compared to future projections, albeit then on their respective native grids as these comparisons are rather between time periods than models. The future time periods are 2037–2063 (mid-century) and 2074–2100 (end of the century). For these two periods, both RCP4.5 and RCP8.5 are analysed (van Vuuren et al., 2011). These represent pathways with stabilization without overshooting to 4.5 W m^{-2} by 2100, and continuous increase to 8.5 W m^{-2} by 2100, respectively.

While the storm track analysis is based on 6-hourly zonal (u) and meridional (v) wind data, sea ice concentration (SIC), sea level pressure (SLP) and total precipitation (hereafter referred to simply as precipitation) examined here are monthly averages. All parameters are analysed over the extended autumn season September through December (SOND), which is the season of greatest ice retreat as shown in Table 1. The seasonal cycle of climatological monthly sea ice extent (SIE) for the previous

decade is captured by the two models, although both models show weaker seasonal cycles of ice
165 retreat compared to the observational data from the National Snow and Ice Data Center (NSIDC;
Fetterer et al., 2002, updated daily) (Table 1). Nevertheless, Langehaug et al. (2013) found the relative trends in NorESM to be close to those observed. In the coming decades, CCSM simulates slightly more rapid ice retreat than NorESM, although both models show the Arctic Ocean becoming seasonally ice-free ($SIE < 1$ million km^2) during the second half of the 21st century (Table 1).
170 The projected reduction of ice extent is greatest in the autumn and early winter, especially in terms of the percentage reduction from the historical values. Even the areal reductions are largest during this portion of the year. Moreover, the observed ice loss during recent decades (1979–present) is also greatest during the autumn (Stroeve et al., 2012; Rogers et al., 2013). In view of this seasonality, we focus our analysis on the SOND season.

175 The storm track analysis is based on the TRACK algorithm described by Hodges (1994, 1995, 1999). It uses 6-hourly 850-hPa relative vorticity (ζ) to identify and track cyclones, here calculated from the u and v fields. Rather than SLP, ζ is used for tracking due to the focus on storminess. ζ contains more information on the wind field and the high-frequency range of the synoptic scale, whereas SLP is linked to the mass field and represents the low-frequency scale better (Hodges et al.,
180 2003). This results in generally more cyclones identified using vorticity tracking (Hodges et al., 2011). Overall, Neu et al. (2013) found the number of storms identified by methods based on vorticity to be in the middle range of those obtained using different tracking algorithms.

The ζ field at moderate to high resolution can nevertheless be very noisy. Hence, to allow the same spatial synoptic scales to be identified in the three data sets, the analysis is performed at a
185 spectral resolution of T42 on a Gaussian grid. Additionally, planetary scales with wave numbers below 5 and above 42 are removed to focus on the synoptic variability. This follows from the data set resolutions and allows some, but not all, polar lows to be resolved (Zappa et al., 2014b). Finally, criteria regarding their displacement distance (minimum 1000 km) and lifetime (minimum 2 days) are set. Only cyclones (not anticyclones) are considered.

190 For this study, two Eulerian statistical fields are of interest: the track density (a relative measure of how many cyclones pass through a region) and the mean intensity (a measure of the strength of the cyclones). These are computed by the spherical kernel estimators described in Hodges (1996). While the mean intensity unit corresponds to relative vorticity (10^{-5} s^{-1}), the track density is given in units of number density per month per unit area, where the unit area is equivalent to a 5° spherical cap
195 ($\sim 10^6 \text{ km}^2$). Although changes of track density also could result from more (less) tightly confined cyclones, they are more likely due to an increase (decrease) in the number of cyclones. Hence, in the following, we refer to changes in the density fields as more or fewer cyclones.

Significance testing of the SIC, SLP and precipitation fields follow the Student's two-sided t -test with a 5 % significance criterion. For the storm track characteristics, p values (the probability
200 that a more extreme value is possible by chance) are computed using a permutation Monte Carlo

approach (sampling without replacement; Hodges, 2008). Correspondingly, grid points with $p < 0.05$ are denoted as significant in storm track figures.

Reanalyses are clearly incapable of capturing mesoscale low pressure systems (including “polar lows”), which have typical scales of 200–300 km and lifetimes generally shorter than two days (Con-
205 dron and Renfrew, 2013). In a comparison of cyclones tracked from the ERA-40 reanalysis and from high-resolution satellite data, Condron et al. (2006) have shown that the failure to capture mesoscale cyclones is especially problematic in the subarctic North Atlantic. The polar low climatologies of Zahn and von Storch (2008) and Bracegirdle and Gray (2008) also show maxima in the subpolar North Atlantic. In the present study, our coarse-resolution models are compared with the coarse-
210 resolution ERA-I reanalysis using the same tracking algorithm, so there is general consistency in the resolution and by implication in the under-capture of cyclones. Nevertheless, the estimates of cyclones reported here from all three sources (ERA-I, NorESM, CCSM) are almost certainly low relative to the actual numbers, and our findings pertain only to systems of synoptic scale and larger.

3 Results and discussion

215 In the following, parameters representing storminess are presented. While Sect. 3.1 compares the representations of NorESM and CCSM to ERA-I, Sect. 3.2 shows the expected changes of these parameters towards the end of the century, as projected by NorESM and CCSM. Only the 2074–2100 time period following the RCP8.5 scenario is shown here because of the near-linear scaling of changes in sea ice, SLP, track density, mean intensity and precipitation with strength of scenario
220 (RCP4.5 and RCP8.5) and time (1979–2005 to 2037–2063 and 2074–2100) in our results (Table 1 and Figs. A to E). Hence, we consider the 2037–2063 time period to be an intermediate state between the historical and 2074–2100 periods, and the RCP4.5 scenario to be mid-way to the RCP8.5 scenario.

While the scaling appear more distinct for sea ice, SLP and precipitation, Figs. C and D show signs
225 of similar behaviour for storm frequency and intensity. This is partly in contrast to Catto et al. (2011). Using the HiGEM high-resolution model, they found northeastward shift of the North Atlantic storm track for the intermediate scenario only. In our results, the northeastward shift gets stronger with scenario and time in NorESM (Figs. Ca to Ce and Figs. Da to De). In CCSM, the North Atlantic storm track generally weakens with scenario and time (Figs. Cf to Cj and Figs. Df to Dj). Overall, signals
230 strengthen with scenario and time in both models. These results extend those of Zappa et al. (2013b), who found mean response generally larger, but also more diverging, for RCP8.5 than RCP4.5 in 19 CMIP5 models (not including CCSM).

Table 2 presents the main results of this study. Representing circumglobal averages spanning large areas, the averages for mid- and high-latitudes might cancel out variations within each region.

235 However, the maps presented in Sects. 3.1 and 3.2 will disclose these features. The values in Table
2 are discussed in more detail in each section.

3.1 Historical time period

3.1.1 Sea level pressure

SLP variations are indirect measures of large-scale storminess. Pressure gradients in space and pres-
240 sure changes for a particular point in time both provide indications of storm activity. The activity
generally increases with decreasing SLP as cyclones lower the SLP of a region as they track through
(Trenberth et al., 2007, and references therein).

Under the assumption that ERA-I represents the actual conditions (Fig. 1a), NorESM and CCSM
reproduce the main SLP pattern (Figs. Ba and Bf), but both also show distinct biases (Figs. 1b
245 and 1c). In midlatitudes (here defined 40–65°N), differences are small, with most of the variations
due to the representation of the Siberian High (Table 2), which is slightly strengthened and shifted
equatorwards in the two models (Fig. 1). This bias is stronger in NorESM, which represents the
Siberian High with SLP up to 1031 hPa compared to the maximum of 1027 hPa in ERA-I.

Contrary to the equatorward-shifted Siberian High, the local minima of the Aleutian and Icelandic
250 lows are shifted polewards in the two models, as represented by the positive (negative) SLP bias
south (north) of the pressure system centres in Fig. 1. This coincides with the marked negative bias
in high-latitudes (here defined 65–90°N) in both models, where NorESM and CCSM depict 2 and 6
hPa, respectively, lower SLP than ERA-I (Table 2 and Figs. 1b and 1c).

The substantial SLP bias in CCSM was also noted by DeWeaver and Bitz (2006), who compared
255 the two resolutions T42 and T85 of CCSM3 (CCSM version 3) to the National Centers for Envi-
ronmental Prediction (NCEP)/NCAR reanalysis. CCSM3 simulated pressures that were too low for
the Aleutian and Icelandic Lows, but with the largest SLP anomalies located over the Beaufort Sea.
They found the bias to be more pronounced in the higher resolution, and ascribed this deficiency
to the model's inability to simulate the Beaufort High in autumn, winter and spring. de Boer et al.
260 (2012) showed that this same bias persists in CCSM4.

3.1.2 Track density

Figures 2a, Ca and Cf shows the distribution in cyclone frequency in the three data sets. The two
main storm tracks of the North Atlantic and the North Pacific oceans are apparent, and likewise the
local maxima over Canada and northern Eurasia.

265 Compared to ERA-I, both models depict poleward-shifted storm tracks over the North Pacific
Ocean, Canadian Arctic and the Nordic Seas (Figs. 2b and 2c). On the contrary, the eastern branch
of the North Atlantic storm track is broader and extends farther south in the models. These features
offer an explanation for the poleward-shifted and wider low SLP bands in Fig. 1. For the North

Atlantic Ocean overall, cyclones in NorESM and CCSM are slightly too zonal compared to ERA-I, consistent with the winter pattern found in CMIP5 models by Zappa et al. (2013a). This leaves fewer cyclones tracking through the Greenland Sea — the region where most Arctic cyclones track (Sorteberg and Walsh, 2008). It is worth mentioning that the zonal North Atlantic storm track bias is stronger in CCSM than in NorESM (Figs. 2b, 2c, Ca and Cc). This coincides with a SIC pattern of higher (lower) SIC in the Labrador Sea (Greenland and Barents seas) in CCSM compared to NorESM (Fig. Af compared to Fig. Aa). This SIE anomaly pattern was also found to be associated with weaker and more zonal North Atlantic storm track in CCSM3 during winter (Magnusdottir et al., 2004).

In CCSM, the number of cyclones within the domain of 40–90°N is 7 % higher than in ERA-I, mainly due to the discrepancy in high-latitudes (Table 2 and Fig. 2c). On the contrary, there are 2 % fewer cyclones in NorESM than found in ERA-I (Table 2 and Fig. 2b). For NorESM, this anomaly stems from its resolution, which is about four times as coarse as in the reanalysis. This leaves fewer cyclones resolved (Hodges et al., 2011).

The signal in CCSM offers an additional explanation to the large-scale background SLP biases across the main storm tracks discussed in Sect. 3.1.1. As more cyclones are resolved in CCSM compared to ERA-I (Table 2), a particular grid point in the main storm track undergoes lower SLP for more time steps, understandably dependent on the cyclone strength. For regions of the main storm tracks, this can lower the SLP temporal mean. This is indicated by the anomalous low SLPs over the poleward-shifted North Atlantic and North Pacific storm tracks (Figs. 1c and 2c). The reason(s) why CCSM gives more cyclones than ERA-I in the first place is (are) unknown, but might reside in its distribution of sea surface temperature or sea ice, or of different parameterization, e.g., for convection.

Moreover, most of the discrepancy relative to ERA-I stems from the high-latitudes south of the Arctic Ocean, with 14 % more cyclones in CCSM over the band 55–65°N (Fig. 2c). This points to a closer similarity of CCSM to the Arctic System Reanalysis (ASR) over ERA-I, as found by Tilinina et al. (2014). They detected 28–40 % more cyclones over high-latitude continental areas in summer and winter in the ASR compared to ERA-I and other global modern era reanalyses, ascribing the anomaly mostly to moderately deep and shallow cyclones (cyclones with central pressure higher than 980 hPa).

3.1.3 Mean intensity

The average strength of cyclones per unit area is presented in Figs. 3a, Da and Df. This is measured as mean intensity, indirectly linked to spatial changes in wind fields through the horizontal component of relative vorticity. Since regions of numerous cyclones are likely also to include more intense cyclones than other regions, the mean intensity pattern generally follows the track density pattern in Figs. 2a, Ca and Cf. Additionally, cyclones are stronger over ocean than land.

305 Corresponding to the general poleward shift of the SLP minima and track density maxima along
the two main storm tracks relative to ERA-I (Figs. 1 and 2), NorESM and CCSM have too low
mean intensities over the North Atlantic and North Pacific oceans (Figs. 3b and 3c). Conversely, as
for track density, positive biases are found over large swaths of Eurasia and western North America,
indicating lower contrasts between regions of high and low cyclonic activity in the models compared
310 to ERA-I (Figs. 2b, 2c, 3b and 3c).

Model biases are generally more coherent for mean intensity than track density (Figs. 3b and
3c compared to Figs. 2b and 2c), where stronger (weaker) cyclones correspond to lower (higher)
SLP (Table 2). However, this relationship does not hold for sea ice-covered areas (Figs. 3b and 3c
compared to Figs. 1b and 1c).

315 In addition to the displacement of the density features in the two models compared to the reanal-
ysis, cyclones are generally weaker in cyclone-dense regions and stronger in cyclone-light regions
(Fig. 3). As with track density (Fig. 2), the values in NorESM are generally lower.

Our results add to the CMIP5 model underestimation of cyclone intensities in the North Atlantic
Ocean in winter and summer compared to ERA-I found by Zappa et al. (2013a). They attributed
320 this bias to either an incorrect representation of dynamical processes on the spatiotemporal scales
of cyclones (e.g., baroclinic conversion, diabatic heating, dissipation) or to biases in the large-scale
processes (e.g., flow-orography interaction, tropical convection, radiative forcing) that determine the
environment in which the cyclones grow. Here, Fig. 3 shows that cyclones are generally weaker in
the two CMIP5 models NorESM and CCSM than ERA-I also in the extended autumn season.

325 **3.1.4 Precipitation**

In terms of broad-scale pattern, precipitation is positively correlated with storminess, although one
cannot say that precipitation is a real measure of storminess. Hawcroft et al. (2012) and Catto et al.
(2012) showed the proportion of precipitation associated with extratropical cyclones and fronts, re-
spectively. Only through this type of linkage can a causal relationship be established. In this study,
330 because precipitation per se is not our main focus, we merely point to consistencies between our
results and general characteristics of precipitation vis-à-vis its drivers. For example, cyclone-dense
regions are generally characterized by high frontal precipitation, with precipitation reaching espe-
cially high levels where cyclones track into mountainous land so that precipitation is orographically
enhanced.

335 Figures 4a, Ea and Ef show the average pattern of precipitation for NH midlatitudes and high-
latitudes over the historical time period. While climate models generally distinguish convective and
non-convective precipitation, their archives do not distinguish frontal and orographic precipitation –
two of the primary types of non-convective precipitation. Nevertheless, one can infer that heavy pre-
cipitation events in non-mountainous areas have a general association with frontal activity (Kunkel
340 et al., 2012), while precipitation maxima in mountainous areas have a substantial orographic com-

ponent. Subject to these assumptions, some inferences can be made about the key features that stand out in Fig. 4.

345 Firstly, frontal precipitation accounts for a large fraction of the precipitation, as seen from the close similarity between the precipitation (Figs. 4a, Ea and Ef) and cyclone track density fields (Figs. 2a, Ca and Cf). Secondly, orographic precipitation is the second most important component to the precipitation. This can be seen from the maxima where the main storm tracks reach land (the west coasts of North America, Scotland and Norway, and the south coasts of Greenland and Iceland in Figs. 4a, Ea and Ef). Moreover, local maxima in connection with the Rocky and Cantabrian mountains, the French and Dinaric alps, as well as Caucasus and the mountains of Japan point to the role of the water bodies to the west of these mountains (Figs. 4a, Ea and Ef). As the westerly wind crosses these waters, the air gains moisture that later result in orographic precipitation on the windward side of the mountains as the air is forced upwards.

355 Frontal precipitation is represented reasonably well in NorESM and CCSM (Figs. Ea and Ef compared to Fig. 4a, and Figs. 4a, Ea and Ef compared to Figs. 2a, Ca and Cf). However, in the North Atlantic Ocean, both models give the precipitation field an orientation that is too zonal in the western half and too meridional in the eastern half. As a consequence, considerably more precipitation falls in the northeastern corner of the North Atlantic Ocean in NorESM and CCSM compared to ERA-I (Figs. 4b and 4c).

The orographic precipitation maxima at storm track landfall in the two models are shifted inland compared to ERA-I (Figs. 4b and 4c). This is likely a result of the resolution difference, in which elevation gradients are smoothed (i.e., weakened) over larger grid boxes. With a prevailing westerly wind in the domain, the air “feels” the mountains later (i.e., farther east) in NorESM and CCSM than in ERA-I. Moreover, the coarse resolution of NorESM restricts the ability to represent orographic precipitation, so the orographic maxima in NorESM are too weak (Fig. 4b).

365 For this reason, and due to the fewer cyclones resolved (Sect. 3.1.2), we would expect to see less precipitation in NorESM than ERA-I. However, the difference over the domain is only a 1 % reduction (Table 2). This might indicate that cyclone frequency has a greater impact on precipitation than cyclone strength, as the corresponding negative biases over the domain for track density and mean intensity are 2 and 5 %, respectively. CCSM, with both more and stronger cyclones, has 10 % more precipitation over the domain than does ERA-I (Table 2).

375 The discussed connection between total precipitation and cyclone frequency and strength is based on an assumption that frontal precipitation is well captured in models. However, Stephens et al. (2010) found that climate models generally overestimate the frequency and underestimate the intensity of precipitation. These compensating errors were discussed in more detail by Catto et al. (2013), who found them largely to be driven by the non-frontal precipitation regimes. These findings are consistent with the biases in NorESM and CCSM.

3.2 Future scenario changes

The following sections outline the projected changes in the four storminess parameters described in Sect. 3.1 over 2074–2100 relative to 1979–2005 following the RCP8.5 scenario in NorESM and
380 CCSM. Rather than seasonal averages as in Table 2 and Figs. 1 to 4, time period averages of the boundary months September and December are given in Table 3 and Figs. 5 to 8. This feature allows a more thorough analysis of expected changes in storminess towards the end of the century in our two models.

In addition to the circumglobal averages over high- and midlatitudes in Table 2, projected changes
385 in track density, mean intensity and precipitation are evaluated for four chosen regions. The regionally averaged parameters are summarized in Table 3 and discussed in Sects. 3.2.2, 3.2.3 and 3.2.4. The regions, pictured in Fig. 6a, were chosen to enable the assessment of a potential shift in the two main historical storm tracks, the North Pacific and North Atlantic storm tracks. The western North America (WNA) and northwestern Europe (NWE) represent the landfall of the main storm
390 tracks in the historical time period, while their northerly neighbouring regions Bering and western Alaska (BWA) and northeastern Europe (NEE) constitute the stormier regions that could result from poleward-shifted storm tracks (see Table 3 for latitudinal and longitudinal boundaries). The four regions have very similar areas and are thus intercomparable.

3.2.1 Sea level pressure

395 Compared to the 1979–2005 historical time period, both models show a significant reduction of 2 hPa in the SLP field over high-latitudes by the end of the century (2074–2100; Table 2 and Fig. 5). We attribute this, at least in part, to the sea ice retreat (Table 1), where most significant reductions occur in regions of sea ice retreat over the century (Fig. 5 and green lines in Fig. 7). With a later refreezing, the autumn air temperatures — although warmer than today (Overland et al., 2013) —
400 create a substantial temperature gradient with the warmer ocean temperature. The result is high heat fluxes from the ocean to the atmosphere, destabilization of the air column and lowered SLP. Baroclinicity is also enhanced by the greater horizontal temperature contrast between land and open ocean during autumn.

Both models also indicate increase in SLP over the North Atlantic Ocean, although more signif-
405 icant in September (Fig. 5). Moreover, they both indicate raised pressures over most of the North Pacific Ocean, with the exception being CCSM in December (Fig. 5). However, due to the significant SLP reduction around the Sea of Okhotsk, especially in December (Figs. 5c and 5d), the average midlatitude changes are negligible (Table 2).

The patterns in Fig. 5 bear resemblance to the positive phase of the Arctic Oscillation (AO). This
410 is indicative of a stronger, less wavy jet stream, which steers storms eastwards to the north of their usual paths and leaves midlatitudes with fewer cold air outbreaks than usual (Thompson and Wallace,

2001). As in other CMIP5 models (Barnes and Polvani, 2013), this pattern is more marked in the North Atlantic compared to the North Pacific sector in NorESM and CCSM.

3.2.2 Track density

415 The variability in the North Pacific storm track severely determines the day-to-day weather conditions downstream in the coastal regions of western Canada and southern Alaska. The same can be said of the North Sea region from the North Atlantic storm track, both regions represented by wet and stormy climates in Figs. 2a, 3a and 4a. This feature explains the choice of regions shown in Fig. 6a. Some earlier studies have indicated poleward shifts of the two main storm tracks in a warmer 420 climate (e.g., Bengtsson et al., 2006, 2009; Fischer-Bruns et al., 2005). If this also holds for NorESM and CCSM, we would expect to see track density reductions in WNA and NWE with corresponding enhancements in BWA and NEE. However, Table 3 shows no clear indications of these shifts.

According to NorESM and CCSM, fewer cyclones will track along the current main storm tracks in the North Atlantic and North Pacific oceans towards the end of the century (Fig. 6). This explains 425 the 3.9 to 6.5 % reductions in midlatitudes found in Table 2, with up to 20.1 % and 21.7 % drops in WNA and NWE activity, respectively (Table 3). On the other hand, there are signals partly indicating more cyclones poleward of this in the two models in Fig. 6.

The general reduction in North Pacific cyclones is associated with more cyclones in parts of the Bering Sea (Fig. 6). However, no consistent tendency is found for the two models and two months, 430 explaining the highly varying changes for BWA in Table 3 (from -13.4% to $+15.5\%$). A comparison to Harvey et al. (2015) reveals that this signal of a poleward shift of the North Pacific storm track was more apparent in CMIP3 models.

NorESM projects a stronger northward shift than CCSM in the North Pacific sector (Figs. 6a and 6c compared to Figs. 6b and 6d), although December averages within the chosen regions suggests 435 the opposite ($+18.2\%$ in WNA, -13.4% in NWE; Table 3). While more cyclones are expected to track through the Bering Strait and into the Arctic Ocean in September, NorESM indicates a more zonal pattern in the North Pacific Ocean for December with a significant increase in a band around 50°N (Figs. 6a and 6c). This pattern is not found in CCSM (Figs. 6b and 6d), which rather projects strong increases along the North American and Siberian Arctic coasts in December (Fig. 6d). The 440 latter feature is mostly a consequence of coinciding enhanced cyclone generation (not shown).

Fewer cyclones track across the North Atlantic Ocean overall in both months and models (Fig. 6). NorESM, like the majority of CMIP5 models (Feser et al., 2015, and references therein), project an eastward extension of the North Atlantic storm track (Figs. 6a and 6c). This evolution occurs downstream of an already too zonal storm track compared to the reanalysis (Fig. 2b), with a 10.2 to 445 12.8 % increase in NWE (Table 3). CCSM too represents the North Atlantic storm track too zonal originally (Fig. 2c), but projects no clear indications of a more zonal storm track towards the end of the 21st century (-21.7 to $+1.2\%$ for NWE in Table 3).

No significant changes are found in NEE (Table 3 and Figs. 6a and 6c). Rather, both NorESM and CCSM show weak reductions in NEE track density (-11.6 to -0.8 %; Table 3) associated with
450 enhancements in the Greenland Sea in September (Figs. 6a and 6b). Fig. A reveals that the latter increase coincides with a sea ice retreat in the Greenland Sea over the century. These results follow those of Deser et al. (2000), Magnusdottir et al. (2004) and Knudsen et al. (2015), who found storm activity to be very sensitive to the sea ice variations east of Greenland. Moreover, Chen et al. (2015) showed a corresponding sensitivity in synoptic activity here associated with variations in the surface
455 mass balance of the Greenland Ice Sheet.

Corresponding to the observed trend found by Sepp and Jaagus (2011), the raised number of cyclones tracking through the Greenland Sea coincides with an increase also in the Labrador Sea and Baffin Bay. While the additional cyclones in these regions are short-lived in CCSM (not shown), they continue polewards (not shown) and add to the projected Arctic Ocean cyclonic activity increase
460 from the Pacific sector in NorESM (Fig. 6a). Nevertheless, this Arctic enhancement is found in September for NorESM alone, and the high-latitude circumglobal changes over the whole season in both models are negligible (-0.8 to $+0.3$ %; Table 2). This contrasts Harvey et al. (2015), who found a significant decrease in high-latitude storm activity with retreating sea ice edge, thus highlighting the complex interconnections determining synoptic changes in a warmer climate system.

Numerous reanalysis studies have shown tendencies of poleward-shifted storm tracks in both the
465 North Atlantic and North Pacific oceans over time (e.g., McCabe et al., 2001; Sepp and Jaagus, 2011; Wang et al., 2006, 2013). Here, only December projections in NorESM resemble similar results. Rather, the general picture of the two main storm tracks in Fig. 6 is more in line with more recent results (e.g., Harvey et al., 2015; Zappa et al., 2013b), with indications of a poleward-shifted North
470 Pacific storm track and eastward-elongated North Atlantic storm track.

3.2.3 Mean intensity

Towards the end of the century, cyclones are generally projected to weaken over midlatitudes (including the main storm tracks) and strengthen over high-latitudes (Table 2 and Fig. 7). This corresponds to the overall picture in Fig. 6, although the high-latitude amplification is clearer for intensities (Table 2). On the other hand, the weakening in midlatitudes is smaller, with an average 2 % reduction
475 in mean intensity over the domain of the two models compared to 4 % decrease in track density. In other words, while there is a projected decrease in number of storms crossing the North Atlantic and the North Pacific oceans, their strength will not drop proportionally. We propose this feature is a result of the overall warming, where higher temperatures and corresponding increases of atmospheric
480 moisture generally favour stronger cyclones.

The results discussed here support the findings of McCabe et al. (2001). They found an insignificant increasing historical trend in winter storm intensity on top of a significant decrease in cyclone frequency over midlatitudes. Moreover, using BCM, Orsolini and Sorteberg (2009) projected a 3.1

to 4.6 % drop in the total number of summer cyclones in the NH over the century, but also saw a
485 slight storm intensification in high-latitudes.

For September, both NorESM and CCSM project a significant increase in cyclone strength over
the Arctic Ocean (Figs. 7a and 7b). By the end of the century, the Arctic is essentially ice-free by
September in NorESM and CCSM (Table 1 and green lines in Figs. 7a and 7b). Hence, as the at-
490 mosphere cools off more rapidly than the ocean in autumn, strong vertical gradients of temperature
and moisture arise. Heat fluxes enter the atmosphere, destabilize the air column and thus foster the
cyclones. Additionally, the enhanced latent heat release and reduced friction (and low-level conver-
gence) due to the sea ice melt might also intensify the cyclones. This intensification might account
in part for the SLP deepening over the Arctic seen in Table 2 and Fig. 5. Stronger cyclones have
lower SLP, and this tendency is consistent with the observational results of Sepp and Jaagus (2011).

495 The heat flux potential is even stronger in December when the temperature gradient between the
ocean and the atmosphere is greater. As a result, the future time period ice-free areas of the Sea
of Okhotsk, Bering and Chukchi seas are projected to be characterized by more intense cyclones
(Figs. 7c and 7d). However, only minor changes are found along the Atlantic sea ice edge, and
NorESM also indicates a significant decrease in cyclone strength over most of the Arctic Ocean (Fig.
500 7c). The latter feature is most likely a result of the significant reduction of the number of cyclones
(Fig. 6c), where the tendency for fewer cyclones is expected to degrade the likelihood of strong
cyclones. Conversely, in the rapidly winter-warming Russian sector (Stocker et al., 2013), cyclones
are projected to become more intense (Figs. 7c and 7d) and, in NorESM, also more numerous (Fig.
6c).

505 According to the two models, cyclones generally weaken in WNA (-6.2 to 0 %) and strengthen
in BWA (-1.4 to $+8.3$ %) in September and December (Table 3 and Fig. 7). This mainly follows
from the poleward-shifted storm track and track density pattern discussed in Sect. 3.2.2, although
the negligible change in cyclone intensity starkly contrasts the 18.2 % increase in cyclone frequency
in WNA for December in NorESM (Table 3) — especially if one would have expanded the region
510 southward. In the coastal regions from Oregon to British Columbia, the number of cyclones sig-
nificantly increases while their strength significantly decreases (Fig. 6c compared to Fig. 7c). The
opposite holds true in BWA (Table 3), demonstrating the closer resemblance between the two models
for mean intensity than track density.

The projected changes in cyclone frequency and intensity along the North American west coast
515 extend the results of Vose et al. (2014). Along this coast, they found a tendency of enhanced cyclonic
activity (number and intensity) in the American sector and reduced activity in the Canadian sector
over 1979–2010 compared to 1948–1978 during the cold season. These tendencies coincided with
raised wave heights from the Baja California peninsula to the Aleutian Islands, emphasizing the
importance of correct cyclone projections with regards to flooding, erosion and coastal activities.

520 In NWE, cyclones weaken by 5.9 to 8.9 % in September and intensify by 1.3 to 4.2 % in December (Table 3). This is indicative of a delayed seasonality, in which the autumn storms in this region come later in the year (not shown). The signal for NEE is less clear, although the changes for the continental areas of the region seem to be anticorrelated with the corresponding continental changes in NWE (Fig. 7).

525 Bengtsson et al. (2006, 2009) found that storms are likely to become less frequent and less intense at midlatitudes, but more numerous and stronger at high-latitudes by the late 21st century compared to the late 20th century. Although mainly focusing on the winter (DJF) and summer (JJA) seasons, the NH averaged signal was also apparent in the autumn (SON) season. Our results in Figs. 6 and 7 strengthen this conclusion, as we would also anticipate a further decrease equatorwards of 40°N.

530 3.2.4 Precipitation

Both models project significantly wetter conditions in high-latitudes by the end of the century compared to the historical time period, with the SOND mean rising 31.8 to 38.2 % (Table 2). As seen in Fig. 8, this applies to both September and December. However, differences between September and December are apparent in midlatitudes. While there is an overall increase also here (8.0 to 10.7
535 %; Table 2), large areas of reduced precipitation occur in September (Figs. 8a and 8b). These are mainly the eastern North Pacific and North Atlantic oceans, the latter giving most of Europe drier conditions by the end of the century.

The reduced precipitation in the eastern North Atlantic Ocean in September coincides with reduced cyclone frequency in CCSM and intensity in both NorESM and CCSM (Figs. 8a and 8b
540 compared to Figs. 6b, 7a and 7b). The correspondence between precipitation and cyclone intensity is consistent with the findings of Zappa et al. (2013b). However, while the changes in storm tracks and precipitation are consistent, this consistency does not prove a causal relationship. The expected drying of the eastern North Atlantic Ocean stems from the poleward migration of the Hadley Cell's downward limb (Kang and Lu, 2012), which is projected to increase dryness in the African-Eurasian
545 region (including the Mediterranean), southwestern North America and northeastern Brazil (Lau and Kim, 2015). The eastern North Atlantic is projected to warm less than the rest of the NH, with relatively lower humidity reducing the potential for increased atmospheric moisture (Stocker et al., 2013). In December, the changes of precipitation in the eastern North Atlantic are mostly positive and are not strongly related to storm track changes (Figs. 8c and 8d).

550 The largest increases in precipitation are found along the shifted main storm tracks and in regions of enhanced cyclone frequency and strength (Figs. 6, 7 and 8), in accordance with the near doubling along the cyclone tracks relative to the global mean increase found by Bengtsson et al. (2009). At the landfall of the shifted storm tracks, western Alaska and northern Scandinavia are projected to see much stormier and wetter autumns by the end of the century (Figs. 6, 7 and 8).

555 Compared to September, the two models predict enhanced precipitation over more of the domain
in December (Figs. 8c and 8d). Part of the reason is that the indication of a poleward shift of the
storm tracks is more significant for September than December (Sects. 3.2.2 and 3.2.3). As in Zappa
et al. (2014a), the expected drier conditions in the Mediterranean region coincide with a reduction in
cyclone frequency (Fig. 6 compared to Fig. 8). This is indicative of the wet-get-wetter, dry-get-drier
560 pattern reported elsewhere (e.g., Held and Soden, 2006; Stocker et al., 2013).

The two models generally agree, but NorESM expands the wetter projection over a larger area
of North America in December (Fig. 8c compared to Fig. 8d). In contrast, the pattern over Europe
shows greater seasonal change in CCSM (Fig. 8d compared to Fig. 8b), with a wider region of
reduced precipitation than in NorESM in September (Fig. 8b compared to Fig. 8a) and a wider
565 region of more precipitation in December (Fig. 8d compared to Fig. 8c). Averaged over the 40–
90°N domain for SOND, the two models both project 0.3 mm d^{-1} more precipitation. This overall
increase of precipitation is consistent with an increase of temperature and the ability of warm air to
contain more moisture, resulting in an acceleration of the hydrologic cycle (Held and Soden, 2006).

Of the four regions, two months and two models in Table 3, only Septembers over the WNA
570 region in NorESM and over the NWE region in CCSM are projected to become drier (4.1 and 12.0
%, respectively). However, compared to the significant increase in precipitation over the domain
(Table 2 and Figs. 8a and 8b), the 5.8 and 5.7 % increases in WNA in CCSM and NWE in NorESM,
respectively, are relatively small, too (Table 3). Again, the poleward-shifted North Pacific and North
Atlantic storm tracks are likely causes, leaving Septembers in the more northern BWA and NEE
575 wetter by 11.7 to 23.8 % (Table 3 and Figs. 6a, 6b, 8a and 8b). More cyclones in the Bering, North
and Greenland seas partly explain the significant increase in precipitation over the continental area
to their east: Alaska, southern and northern Norway (Figs. 6a, 6b, 8a and 8b).

In December, the poleward storm track shift is less significant (Figs. 6c and 6d), giving 8.7 to
19.7 % more precipitation in WNA and NWE (Table 3 and Figs. 8c and 8d). The models still project
580 significantly wetter conditions in BWA and NEE (although with an exception of NEE in CCSM;
Fig. 8d), highlighting the increased availability of warmer air to hold moisture in the most rapidly
warming region and season (Stocker et al., 2013).

Totalled over the full season SOND, the projected changes in precipitation in Fig. 8 might have
severe consequences for multiple regions. Two of these are the Norwegian west coast (here defined
585 $58\text{--}63^\circ\text{N}$, $5.0\text{--}7.5^\circ\text{E}$) and the Gulf of Alaska (here defined $58\text{--}63^\circ\text{N}$, $135\text{--}155^\circ\text{W}$). They are cur-
rently among the wettest regions in the extratropical NH. If we would believe the projections from
the models, an additional 39 (CCSM) to 132 mm (NorESM) and 71 (NorESM) to 115 mm (CCSM)
precipitation will fall over the Norwegian west coast and the Gulf of Alaska, respectively, over each
SOND season during the years 2074–2100 compared to 1979–2005.

590 4 Conclusions

In this study, we have used a vorticity-based storm-tracking algorithm to analyse changes in metrics of storminess in high- and midlatitudes through 2100 in the NorESM1-M global climate model. The main findings obtained from NorESM1-M are generally supported by the results obtained from a second model, CCSM4, which was examined for comparison purposes. The two models were also
595 compared to the reanalysis data set ERA-Interim for the historical time period. Results are based on only one ensemble member for each model due to the required tracking method criteria.

The primary findings include the following:

- 600 – The ongoing and projected retreat of sea ice is greatest in autumn, creating the potential for increased fluxes of sensible and latent heat to from the surface to the atmosphere during these months.
- The models reproduce the observed seasonality of the sea ice loss and the general patterns of sea level pressure (SLP) and cyclone metrics, although the storm tracks (densities) and intensities are somewhat less sharp relative to ERA-I because of the models' coarser resolution.
- 605 – For the two models (with one ensemble member each), the projected changes in storm intensity (as well as sea ice, SLP and precipitation) appear to scale generally linearly with the RCP value of the forcing scenario and with time through the 21st century.
- 610 – A significant projected decrease of the SLP over the Arctic Ocean during the 21st century appears to be partly a consequence of the diminishing sea ice cover on the same time scales. These changes are consistent with increased heating of the lower troposphere over areas of sea ice loss, resulting in increased thicknesses in the lower troposphere, and increased geopotential heights and mass divergence aloft. Accordingly, sea level pressures are projected to decrease over the Arctic Ocean and increase farther south, significantly over the North Atlantic Ocean, coinciding with reduced midlatitude storm track activity.
- 615 – Cyclones are generally expected to weaken over midlatitudes and strengthen over high-latitudes, although this is more apparent for September than December. The intensification is especially marked in areas of sea ice retreat, where cyclones foster from heat fluxes into the atmosphere, latent heat release and reduced friction.
- 620 – Projected changes in track density are much less coherent, although there is a general tendency towards less frequent storms in midlatitudes and more frequent storms in certain regions at high-latitudes. Relatively large increases in frequency are projected locally for the Baffin Bay/Davis Strait region in September.
- Over the whole domain circumpolar north of 40°N, there is a tendency of slightly fewer and weaker cyclones towards the end of the century. However, the reduction in frequency (4 %)

625 is larger than intensity (2 %), indicating that changes in cyclone strength do not correlate proportionally to cyclone frequency.

- Autumn precipitation is projected to increase significantly across the entire high-latitudes. Together with the projected increases in storm intensity and sea level and the loss of sea ice, this increase implies a greater vulnerability to coastal flooding and erosion, especially in the Alaskan region.

630 The results reported here are limited to two climate models and to two simulations by each model, one with a low emission scenario (RCP 4.5) and one with a high (business-as-usual) scenario (RCP 8.5). The projected changes appear to scale linearly with the intensity of the RCP forcing. The robustness of such results obtained would be enhanced by the inclusion of additional models and ensemble members. However, the results obtained from the two different models show enough similarities that
635 the conclusions listed above can be taken as starting points in assessments of the likely changes in storm activity in the northern high-latitudes.

As additional models and ensemble members are included in assessments of future changes in Arctic cyclone activity, the relative importance of internal variability (deduced from different ensemble members of a single model) and model-derived uncertainty (deduced from across-model
640 differences in cyclone statistics) will be important to an assessment of uncertainties. Should across-model differences dominate (as they do with temperature, for example), priority must be given to diagnosing the reasons why the models are different. It may also be fruitful to explore model selection (“filtering”) strategies based on the fidelity of the models to the observed data on cyclone activity.

645 Storm frequency, intensity and precipitation changes are likely to have costly impacts on human society, especially on top of sea level rise. This adds to the importance of reducing the uncertainties in future changes of Arctic cyclone activity and related variables that will impact northern coasts, communities and offshore activities.

Appendix A: Author contribution

650 The authors shared the task of designing and evaluating the study, while E.M. Knudsen carried out the data acquisition and analysis. E.M. Knudsen also prepared the manuscript, but with significant contributions from J.E. Walsh.

Appendix B: Additional figures

Acknowledgements. We thank K.I. Hodges for providing the TRACK algorithm and guidance on p-value calculations for the storm track parameters. We are grateful to A. Sorteberg for his helpful internal review of an earlier
655

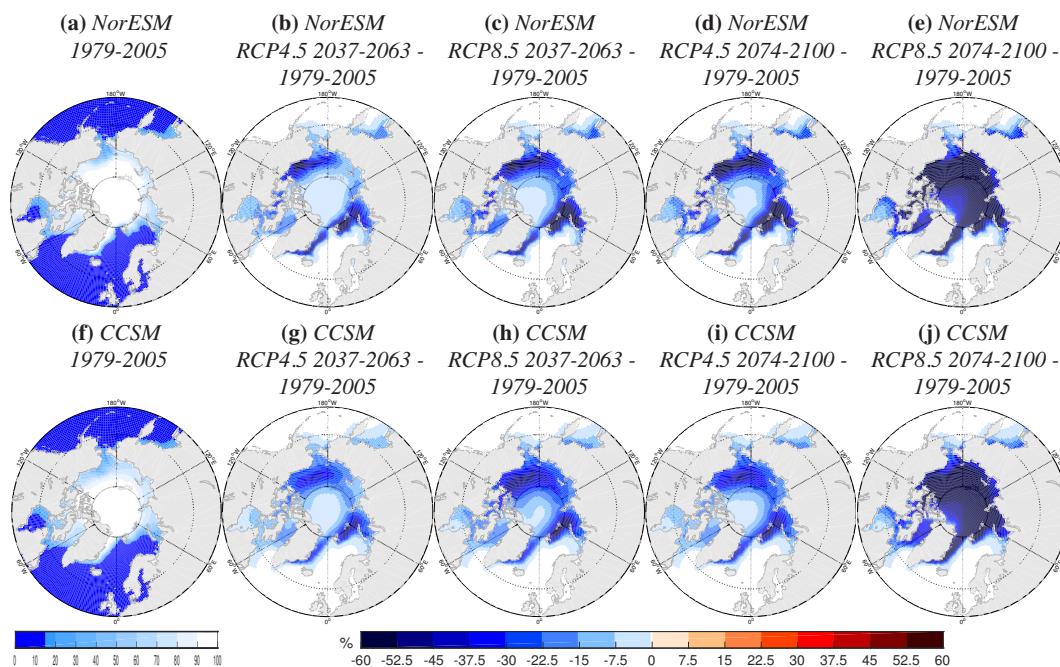


Figure A. Sea ice concentration (a), (f) averages for SONDJ 1979–2005 and (b), (c), (d), (e), (g), (h), (i), (j) changes in average over various time periods and scenarios relative to 1979–2005 in NorESM (upper row) and CCSM (lower row). The time periods and scenarios are (b), (g) RCP4.5 2037–2063 – 1979–2005, (c), (h) RCP8.5 2037–2063 – 1979–2005, (d), (i) RCP4.5 2074–2100 – 1979–2005 and (e), (j) RCP8.5 2074–2100 – 1979–2005.

version of this manuscript. We also wish to thank the two anonymous reviewers who provided constructive suggestions that improved the manuscript. The data for this paper are available at Program for Climate Model Diagnosis and Intercomparison’s web page CMIP5 Coupled Model Intercomparison Project (<http://cmip-pcmdi.llnl.gov/cmip5/index.html>) and at ECMWF’s ERA-I web access (http://apps.ecmwf.int/datasets/data/interim_full_moda/). The work was financially supported by the Research Council of Norway through the BlueArc project (no. 207650) and by the U.S. National Science Foundation through Grants ARC-1023131 and ARC-1049225.

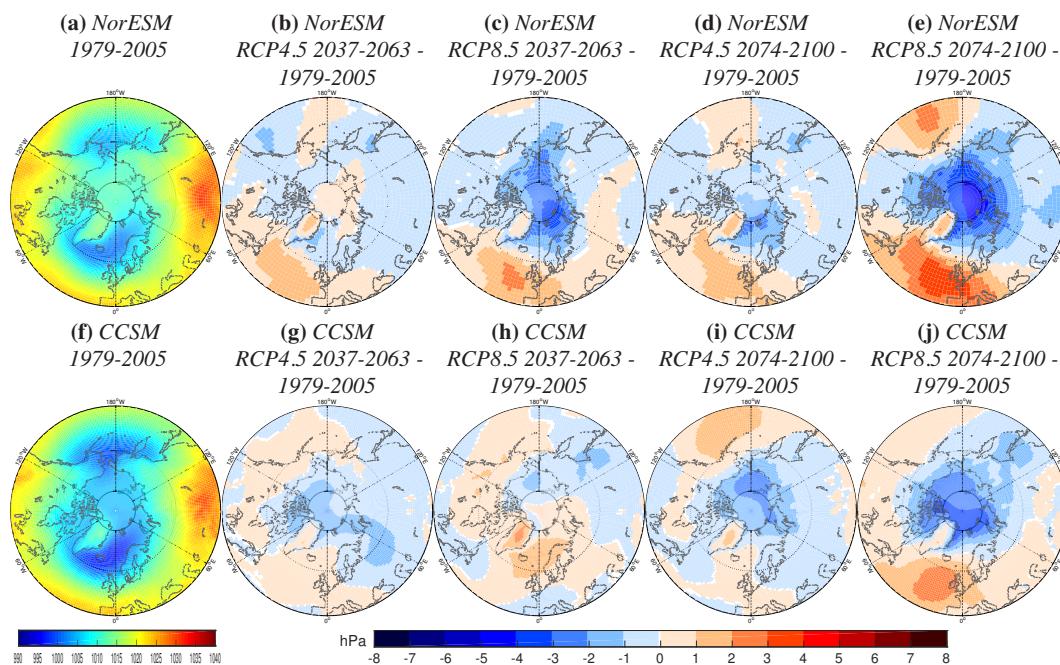


Figure B. Sea level pressure (a), (f) averages for SOND 1979–2005 and (b), (c), (d), (e), (g), (h), (i), (j) changes in average over various time periods and scenarios relative to 1979–2005 in NorESM (upper row) and CCSM (lower row). The time periods and scenarios are (b), (g) RCP4.5 2037–2063 – 1979–2005, (c), (h) RCP8.5 2037–2063 – 1979–2005, (d), (i) RCP4.5 2074–2100 – 1979–2005 and (e), (j) RCP8.5 2074–2100 – 1979–2005.

References

- AMAP: Arctic Climate Impact Assessment (ACIA), Tech. rep., Arctic Monitoring and Assessment Programme (AMAP), New York, USA, 2005.
- 665 AMAP: Snow, water, ice and permafrost in the Arctic (SWIPA): Climate change and the cryosphere, Tech. rep., Arctic Monitoring and Assessment Programme (AMAP), Oslo, Norway, 2011.
- Barnes, E.: Revisiting the evidence linking Arctic amplification to extreme weather in midlatitudes, *Geophys. Res. Lett.*, 40, 4734–4739, doi:10.1002/grl.50880, 2013.
- 670 Barnes, E. and Polvani, L.: Response of the midlatitude jets, and of their variability, to increased greenhouse gases in the CMIP5 models, *J. Climate*, 26, 7117–7135, doi:10.1175/JCLI-D-12-00536.1, 2013.
- Barnes, E. and Screen, J.: The impact of Arctic warming on the midlatitude jet-stream: Can it? Has it? Will it?, *WIREs Clim. Change*, 6, 277–286, doi:10.1002/wcc.337, 2015.
- Barnes, E., Dunn-Sigouin, E., Masato, G., and Woollings, T.: Exploring recent trends in Northern Hemisphere blocking, *Geophys. Res. Lett.*, 41, 638–644, doi:10.1002/2013GL058745, 2014.
- 675 Bekryaev, R., Polyakov, I., and Alexeev, V.: Role of polar amplification in long-term surface air temperature variations and modern Arctic warming, *J. Climate*, 23, 3888–3906, doi:10.1175/2010JCLI3297.1, 2010.
- Bengtsson, L., Hodges, K., and Roeckner, E.: Storm tracks and climate change, *J. Climate*, 19, 3518–3543, doi:10.1175/JCLI3815.1, 2006.

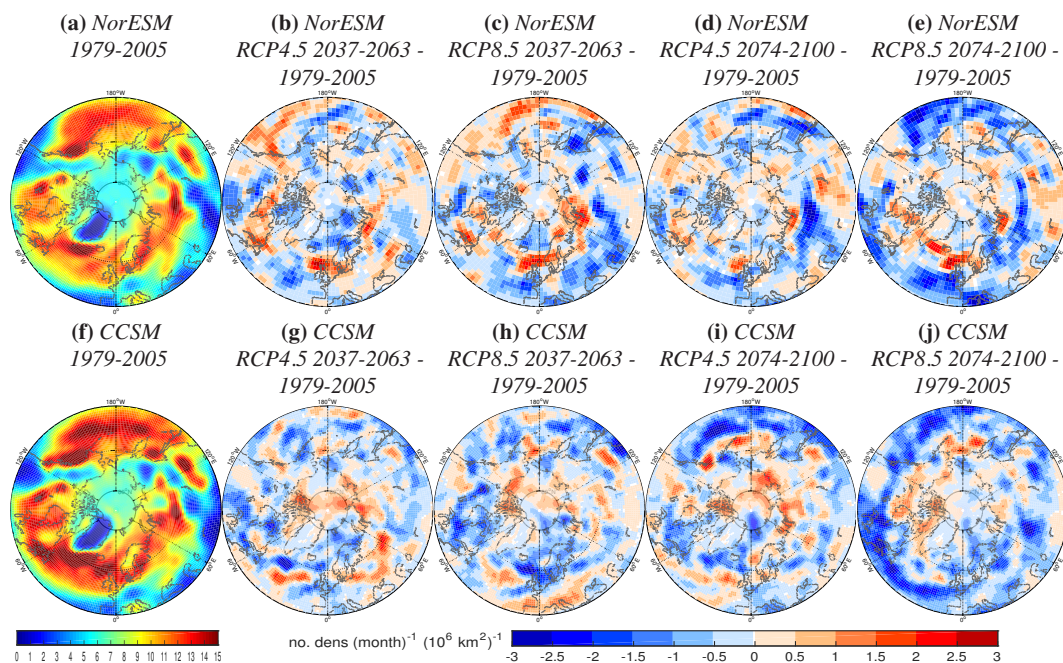


Figure C. Track density (a), (f) averages for SONDJ 1979–2005 and (b), (c), (d), (e), (g), (h), (i), (j) changes in average over various time periods and scenarios relative to 1979–2005 in NorESM (upper row) and CCSM (lower row). The time periods and scenarios are (b), (g) RCP4.5 2037–2063 – 1979–2005, (c), (h) RCP8.5 2037–2063 – 1979–2005, (d), (i) RCP4.5 2074–2100 – 1979–2005 and (e), (j) RCP8.5 2074–2100 – 1979–2005.

680 Bengtsson, L., Hodges, K., and Keenlyside, N.: Will extratropical storms intensify in a warmer climate?, *J. Climate*, 22, 2276–2301, doi:10.1175/2008JCLI2678.1, 2009.

Bentsen, M., Bethke, I., Debernard, J., Iversen, T., Kirkevåg, A., Seland, Ø., Drange, H., Roelandt, C., Seierstad, I., Hoose, C., and Kristjánsson, J.: The Norwegian Earth System Model, NorESM1-M — Part 1: Description and basic evaluation of the physical climate, *Geosci. Model Dev.*, 6, 687–720, doi:10.5194/gmd-6-687-2013, 685 2013.

Bleck, R., Rooth, C., Hu, D., and Smith, L.: Salinity-driven thermocline transients in a wind-and thermohaline-forced isopycnic coordinate model of the North Atlantic, *J. Phys. Oceanogr.*, 22, 1486–1505, doi:10.1175/1520-0485(1992)022<1486:SDTTIA>2.0.CO;2, 1992.

Bracegirdle, T. and Gray, S.: An objective climatology of the dynamical forcing of polar lows in the Nordic 690 Seas, *Int. J. Climatol.*, 28, 1903–1919, doi:10.1002/joc.1686, 2008.

Catto, J., Shaffrey, L., and Hodges, K.: Northern Hemisphere extratropical cyclones in a warming climate in the HiGEM high-resolution climate model, *J. Climate*, 24, 5336–5352, doi:10.1175/2011JCLI4181.1, 2011.

Catto, J., Jakob, C., Berry, G., and Nicholls, N.: Relating global precipitation to atmospheric fronts, *Geophys. Res. Lett.*, 39, L10 805, doi:10.1029/2012GL051736, 2012.

695 Catto, J., Jakob, C., and Nicholls, N.: A global evaluation of fronts and precipitation in the ACCESS model, *Aust. Meteorol. Ocean. Soc. J.*, 63, 191–203, 2013.

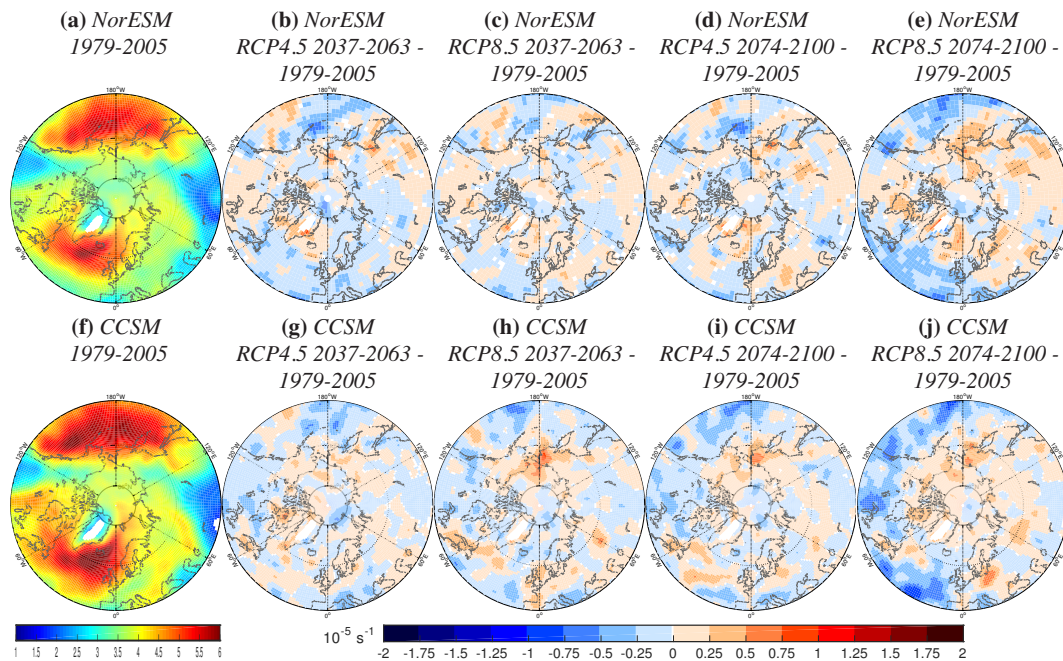


Figure D. Mean intensity (a), (f) averages for SOND 1979–2005 and (b), (c), (d), (e), (g), (h), (i), (j) changes in average over various time periods and scenarios relative to 1979–2005 in NorESM (upper row) and CCSM (lower row). The time periods and scenarios are (b), (g) RCP4.5 2037–2063 – 1979–2005, (c), (h) RCP8.5 2037–2063 – 1979–2005, (d), (i) RCP4.5 2074–2100 – 1979–2005 and (e), (j) RCP8.5 2074–2100 – 1979–2005. Regions with track density below 0.5 no. density (month)^{−1} (10⁶ km²)^{−1} in the historical time period are shaded white.

Chen, L., Fettweis, X., Knudsen, E., and Johannessen, O.: Impact of cyclonic and anticyclonic activity on Greenland ice sheet surface mass balance variation during 1980–2013, *Int. J. Climatol.*, doi:10.1002/joc.4565, 2015.

700 Chung, C., Cha, H., Vihma, T., Räisänen, P., and Decremier, D.: On the possibilities to use atmospheric reanalyses to evaluate the warming structure in the Arctic, *Atmos. Chem. Phys.*, 13, 11 209–11 219, doi:10.5194/acp-13-11209-2013, 2013.

Cohen, J., Furtado, J., Barlow, M., Alexeev, V., and Cherry, J.: Arctic warming, increasing snow cover and widespread boreal winter cooling, *Environ. Res. Lett.*, 7, 014 007, doi:10.1088/1748-9326/7/1/014007, 2012.

705 Condron, A. and Renfrew, I.: The impact of polar mesoscale storms on northeast Atlantic Ocean circulation, *Nat. Geosci.*, 6, 34–37, doi:10.1038/ngeo1661, 2013.

Condron, A., Bigg, G., and Renfrew, I.: Polar mesoscale cyclones in the northeast Atlantic: Comparing climatologies from ERA-40 and satellite imagery, *Mon. Weather Rev.*, 134, 1518–1533, doi:10.1175/MWR3136.1, 2006.

710 de Boer, G., Chapman, W., Kay, J., Medeiros, B., Shupe, M., Vavrus, S., and Walsh, J.: A characterization of the present-day Arctic atmosphere in CCSM4, *J. Climate*, 25, 2676–2695, doi:10.1175/JCLI-D-11-00228.1, 2012.

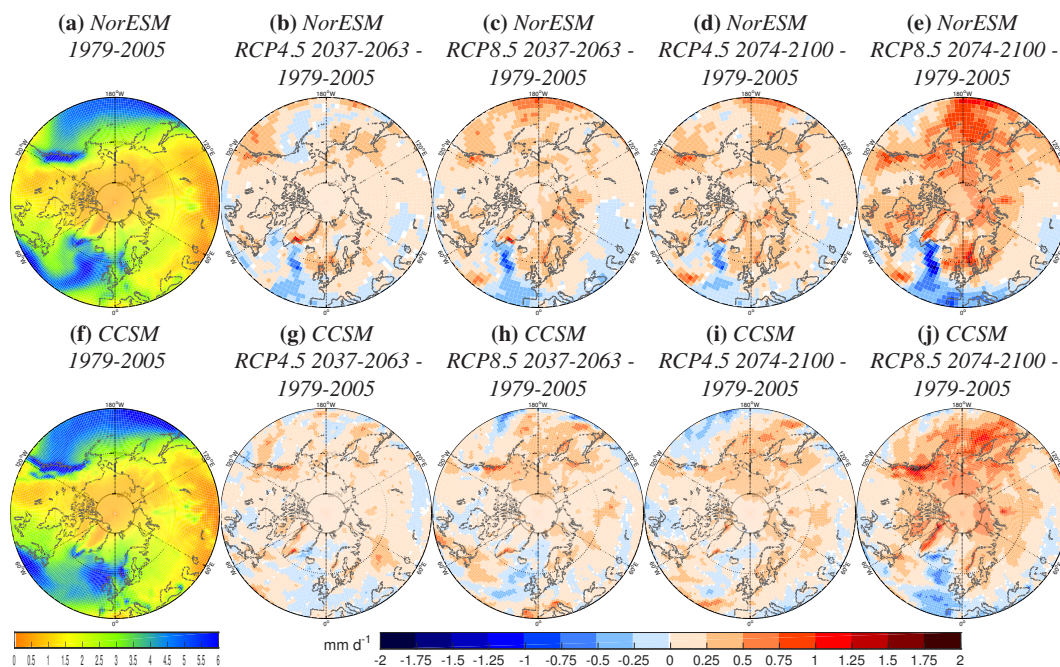


Figure E. Precipitation (a), (f) averages for SOND 1979–2005 and (b), (c), (d), (e), (g), (h), (i), (j) changes in average over various time periods and scenarios relative to 1979–2005 in NorESM (upper row) and CCSM (lower row). The time periods and scenarios are (b), (g) RCP4.5 2037–2063 – 1979–2005, (c), (h) RCP8.5 2037–2063 – 1979–2005, (d), (i) RCP4.5 2074–2100 – 1979–2005 and (e), (j) RCP8.5 2074–2100 – 1979–2005.

Dee, D., Uppala, S., Simmons, A., Berrisford, P., Poli, P., Kobayashi, S., Andrae, U., Balmaseda, M., Balsamo, G., Bauer, P., Bechtold, P., Beljaars, A., van de Berg, L., Bidlot, J., Bormann, N., Delsol, C., Dragani, R.,
715 Fuentes, M., Geer, A., Haimberger, L., Healy, S., Hersbach, H., Hólm, E., Isaksen, L., Kållberg, P., Köhler, M., Matricardi, M., McNally, A., Monge-Sanz, B., Morcrette, J.-J., Park, B.-K., Peubey, C., de Rosnay, P., Tavolato, C., Thépaut, J.-N., and Vitart, F.: The ERA-Interim reanalysis: Configuration and performance of the data assimilation system, *Q. J. Roy. Meteor. Soc.*, 137, 553–597, doi:10.1002/qj.828, 2011.

Deser, C., Walsh, J., and Timlin, M.: Arctic sea ice variability in the context of recent atmospheric circulation trends, *J. Climate*, 13, 617–633, doi:10.1175/1520-0442(2000)013<0617:ASIVIT>2.0.CO;2, 2000.

DeWeaver, E. and Bitz, C.: Atmospheric circulation and its effect on Arctic sea ice in CCSM3 simulations at medium and high resolution, *J. Climate*, 19, 2415–2436, doi:10.1175/JCLI3753.1, 2006.

Drange, H., Gerdes, R., Gao, Y., Karcher, M., Kauker, F., and Bentsen, M.: Ocean general circulation modelling of the Nordic Seas, in: *The Nordic Seas: An integrated perspective*, edited by Drange, H., Dokken, T., Furevik, T., Gerdes, R., and Berger, W., vol. 158, pp. 199–219, Wiley Online Library, Washington D.C., USA,
725 2005.

Feser, F., Barcikowska, M., Krueger, O., Schenk, F., Weisse, R., and Xia, L.: Storminess over the North Atlantic and northwestern Europe — A review, *Q. J. Roy. Meteor. Soc.*, 141, 350–382, doi:10.1002/qj.2364, 2015.

Fetterer, F., Knowles, K., Meier, W., and Savoie, M.: Sea Ice Index, Version 1, doi:10.7265/N5QJ7F7W, digital
730 media, 2002, updated daily.

Fischer-Bruns, I., von Storch, H., González-Rouco, J., and Zorita, E.: Modelling the variability of midlatitude
storm activity on decadal to century time scales, *Clim. Dynam.*, 25, 461–476, doi:10.1007/s00382-005-0036-
1, 2005.

Francis, J. and Vavrus, S.: Evidence linking Arctic amplification to extreme weather in mid-latitudes, *Geophys.*
735 *Res. Lett.*, 39, L06 801, doi:10.1029/2012GL051000, 2012.

Furevik, T., Bentsen, M., Drange, H., Kindem, I., Kvamstø, N., and Sorteberg, A.: Description and evaluation of
the Bergen climate model: ARPEGE coupled with MICOM, *Clim. Dynam.*, 21, 27–51, doi:10.1007/s00382-
003-0317-5, 2003.

Gent, P., Danabasoglu, G., Donner, L., Holland, M., Hunke, E., Jayne, S., Lawrence, D., Neale, R., Rasch, P.,
740 Vertenstein, M., Worley, P., Yang, Z.-L., and Zhang, M.: The Community Climate System Model version 4,
J. Climate, 24, 4973–4991, doi:10.1175/2011JCLI4083.1, 2011.

Harvey, B., Shaffrey, L., and Woollings, T.: Deconstructing the climate change response of the Northern Hemi-
sphere wintertime storm tracks, *Clim. Dynam.*, 45, 2847–2860, doi:10.1007/s00382-015-2510-8, 2015.

Hawcroft, M., Shaffrey, L., Hodges, K., and Dacre, H.: How much Northern Hemisphere precipitation is asso-
745 ciated with extratropical cyclones?, *Geophys. Res. Lett.*, 39, L24 809, doi:10.1029/2012GL053866, 2012.

Held, I. and Soden, B.: Robust responses of the hydrological cycle to global warming, *J. Climate*, 19, 5686–
5699, doi:10.1175/JCLI3990.1, 2006.

Hodges, K.: A general method for tracking analysis and its application to meteorological data, *Mon. Weather*
Rev., 122, 2573–2586, doi:10.1175/1520-0493(1994)122<2573:AGMFTA>2.0.CO;2, 1994.

750 Hodges, K.: Feature tracking on the unit-sphere, *Mon. Weather Rev.*, 123, 3458–3465, doi:10.1175/1520-
0493(1995)123<3458:FTOTUS>2.0.CO;2, 1995.

Hodges, K.: Spherical nonparametric estimators applied to the UGAMP model integration for AMIP, *Mon.*
Weather Rev., 124, 2914–2932, doi:10.1175/1520-0493(1996)124<2914:SNEATT>2.0.CO;2, 1996.

Hodges, K.: Adaptive constraints for feature tracking, *Mon. Weather Rev.*, 127, 1362–1373, doi:10.1175/1520-
755 0493(1999)127<1362:ACFFT>2.0.CO;2, 1999.

Hodges, K.: Confidence intervals and significance tests for spherical data derived from feature tracking, *Mon.*
Weather Rev., 136, 1758–1777, doi:10.1175/2007MWR2299.1, 2008.

Hodges, K., Hoskins, B., Boyle, J., and Thorncroft, C.: A comparison of recent reanalysis datasets using ob-
jective feature tracking: Storm tracks and tropical easterly waves, *Mon. Weather Rev.*, 131, 2012–2037,
760 doi:10.1175/1520-0493(2003)131<2012:ACORRD>2.0.CO;2, 2003.

Hodges, K., Lee, R., and Bengtsson, L.: A comparison of extratropical cyclones in recent re-
analyses ERA-Interim, NASA MERRA, NCEP CFSR, and JRA-25, *J. Climate*, 24, 4888–4906,
doi:10.1175/2011JCLI4097.1, 2011.

Iversen, T., Bentsen, M., Bethke, I., Debernard, J., Kirkevåg, A., Seland, Ø., Drange, H., Kristjánsson, J., Med-
765 haug, I., Sand, M., and Seierstad, I.: The Norwegian Earth System Model, NorESM1-M — Part 2: Climate
response and scenario projections, *Geosci. Model Dev.*, 6, 389–415, doi:10.5194/gmd-6-389-2013, 2013.

Jakobson, E., Vihma, T., Palo, T., Jakobson, L., Keernik, H., and Jaagus, J.: Validation of atmospheric reanalyses
over the central Arctic Ocean, *Geophys. Res. Lett.*, 39, L10 802, doi:10.1029/2012GL051591, 2012.

770 Kang, S. and Lu, J.: Expansion of the Hadley cell under global warming: Winter versus summer, *J. Climate*, 25,
8387–8393, doi:10.1175/JCLI-D-12-00323.1, 2012.

Karl, T., Melillo, J., Peterson, T., and (eds.): Global climate change impacts in the United States, Tech. rep.,
U.S. Global Change Research Program (USGRP), Cambridge, United Kingdom and New York, USA, 2009.

775 Kirkevåg, A., Iversen, T., Seland, Ø., Hoose, C., Kristjánsson, J., Struthers, H., Ekman, A., Ghan, S., Gries-
feller, J., Nilsson, E., and Schulz, M.: Aerosol-climate interactions in the Norwegian Earth System Model —
NorESM1-M, *Geosci. Model Dev.*, 6, 207–244, doi:10.5194/gmd-6-207-2013, 2013.

Knudsen, E., Orsolini, Y., Furevik, T., and Hodges, K.: Observed anomalous atmospheric patterns in summers
of unusual Arctic sea ice melt, *J. Geophys. Res.-Atmos.*, 120, 2595–2611, doi:10.1002/2014JD022608, 2015.

Kunkel, K., Easterling, D., Kristovich, D., Gleason, B., Stoecker, L., and Smith, R.: Meteorological causes
of the secular variations in observed extreme precipitation events for the conterminous United States, *J.*
780 *Hydrometeorology*, 13, 1131–1141, doi:10.1175/JHM-D-11-0108.1, 2012.

Kuo, Y.-H., Shapiro, M., and Donall, E.: The interaction between baroclinic and diabatic processes in a numeri-
cal simulation of a rapidly intensifying extratropical marine cyclone, *Mon. Weather Rev.*, 119, 368–384,
doi:10.1175/1520-0493(1991)119<0368:TIBBAD>2.0.CO;2, 1991.

Langehaug, H., Geyer, F., Smedsrud, L., and Gao, Y.: Arctic sea ice decline and ice export in the CMIP5
785 historical simulations, *Ocean Modelling*, 71, 114–126, doi:10.1016/j.ocemod.2012.12.006, 2013.

Lau, W. and Kim, K.-M.: Robust Hadley Circulation changes and increasing global dryness due
to CO₂ warming from CMIP5 model projections, *P. Natl. Acad. Sci. USA*, 112, 3630–3635,
doi:10.1073/pnas.1418682112, 2015.

Long, Z. and Perrie, W.: Air-sea interactions during an Arctic storm, *J. Geophys. Res.-Atmos.*, 117, D15 103,
790 doi:10.1029/2011JD016985, 2012.

Lynch, A., Cassano, E., Cassano, J., and Lestak, L.: Case studies of high wind events in Barrow, Alaska:
Climatological context and development processes, *Mon. Weather Rev.*, 131, 719–732, doi:10.1175/1520-
0493(2003)131<0719:CSOHWE>2.0.CO;2, 2003.

Magnusdottir, G., Deser, C., and Saravanan, R.: The effects of North Atlantic SST and sea ice anomalies on the
795 winter circulation in CCM3. Part I: Main features and storm track characteristics of the response, *J. Climate*,
17, 857–876, doi:10.1175/1520-0442(2004)017<0857:TEONAS>2.0.CO;2, 2004.

Maier-Reimer, E.: Geochemical cycles in an ocean general circulation model. Preindustrial tracer distributions,
Global Biogeochem. Cy., 7, 645–677, doi:10.1029/93GB01355, 1993.

Maier-Reimer, E., Kriest, I., Segschneider, J., and Wetzol, P.: The HAMBURG Ocean Carbon Cycle Model
800 HAMOCC 5.1 — Technical description release 1.1, Tech. rep., Max Planck Institute for Meteorology, Ham-
burg, Germany, 2005.

McCabe, G., Clark, M., and Serreze, M.: Trends in Northern Hemisphere surface cyclone frequency and inten-
sity, *J. Climate*, 14, 2763–2768, doi:10.1175/1520-0442(2001)014<2763:TINHSC>2.0.CO;2, 2001.

Melillo, J., Richmond, T., Yohe, G., and (eds.): Climate change impacts in the United States, Tech. rep., U.S.
805 Global Change Research Program (USGRP), Washington D.C., USA, 2014.

Mesquita, M., Atkinson, D., and Hodges, K.: Characteristics and variability of storm tracks in the North Pacific,
Bering Sea, and Alaska*, *J. Climate*, 23, 294–311, doi:10.1175/2009JCLI3019.1, 2010.

- Neu, U., Akperov, M., Bellenbaum, N., Benestad, R., Blender, R., Caballero, R., Coccozza, A., Dacre, H., Feng, Y., Fraedrich, K., Grieger, J., Gulev, S., Hanley, J., Hewson, T., Inatsu, M., Keay, K., Kew, S., Kindem, I.,
810 Leckebusch, G., Liberato, M., Lionello, P., Mokhov, I., Pinto, J., Raible, C., Reale, M., Rudeva, I., Schuster, M., Simmonds, I., Sinclair, M., Sprenger, M., Tilinina, N., Trigo, I., Ulbrich, S., Ulbrich, U., Wang, X., and Wernli, H.: IMILAST: A community effort to intercompare extratropical cyclone detection and tracking algorithms, *B. Am. Meteorol. Soc.*, 94, 529–547, doi:10.1175/BAMS-D-11-00154.1, 2013.
- Orsolini, Y. and Sorteberg, A.: Projected changes in Eurasian and Arctic summer cyclones under global warm-
815 ing in the Bergen Climate Model, *Atmos. Oceanic Sci. Lett.*, 2, 62–67, 2009.
- Overland, J. and Wang, M.: Large-scale atmospheric circulation changes are associated with the recent loss of Arctic sea ice, *Tellus A*, 62, 1–9, doi:10.1111/j.1600-0870.2009.00421.x, 2010.
- Overland, J., Wang, M., Walsh, J., and Stroeve, J.: Future Arctic climate changes: Adaptation and mitigation time scales, *Earth’s Future*, 2, 68–74, doi:10.1002/2013EF000162, 2013.
- 820 Pithan, F. and Mauritsen, T.: Arctic amplification dominated by temperature feedbacks in contemporary climate models, *Nat. Geosci.*, 7, 181–184, doi:10.1038/ngeo2071, 2014.
- Rogers, T., Walsh, J., Rupp, T., Brigham, L., and Sfraga, M.: Future Arctic marine access: Analysis and evaluation of observations, models, and projections of sea ice, *The Cryosphere*, 7, 321–332, doi:10.5194/tc-7-321-2013, 2013.
- 825 Screen, J. and Simmonds, I.: Exploring links between Arctic amplification and mid-latitude weather, *Geophys. Res. Lett.*, 40, 959–964, doi:10.1002/GRL.50174, 2013.
- Sepp, M. and Jaagus, J.: Changes in the activity and tracks of Arctic cyclones, *Climatic Change*, 105, 577–595, doi:10.1007/s10584-010-9893-7, 2011.
- Simmonds, I. and Keay, K.: Extraordinary September Arctic sea ice reductions and their relationships with
830 storm behavior over 1979–2008, *Geophys. Res. Lett.*, 36, L19 715, doi:10.1029/2009GL039810, 2009.
- Simmonds, I. and Rudeva, I.: The great Arctic cyclone of August 2012, *Geophys. Res. Lett.*, 39, L23 709, doi:10.1029/2012GL054259, 2012.
- Sorteberg, A. and Walsh, J.: Seasonal cyclone variability at 70°N and its impact on moisture transport into the Arctic, *Tellus A*, 60, 570–586, doi:10.1111/j.1600-0870.2008.00314.x, 2008.
- 835 Stephens, G., L’Ecuyer, T., Forbes, R., Gettleman, A., Golaz, J.-C., Bodas-Salcedo, A., Suzuki, K., Gabriel, P., and Haynes, J.: Dreary state of precipitation in global models, *J. Geophys. Res.-Atmos.*, 115, D24 211, doi:10.1029/2010JD014532, 2010.
- Stocker, T., Qin, D., Plattner, G.-K., Tignor, M., Allen, S., Boschung, J., Nauels, A., Xia, Y., V. B., Midgley, P., and (eds.): Climate change 2013: The physical science basis. Contribution of Working Group I to the Fifth
840 Assessment Report of the Intergovernmental Panel on Climate Change, Tech. rep., Intergovernmental Panel on Climate Change (IPCC), Cambridge, United Kingdom and New York, USA, 2013.
- Stroeve, J., Kattsov, V., Barrett, A., Serreze, M., Pavlova, T., Holland, M., and Meier, W.: Trends in Arctic sea ice extent from CMIP5, CMIP3 and observations, *Geophys. Res. Lett.*, 39, L16 502, doi:10.1029/2012GL052676, 2012.
- 845 Taylor, K., Stouffer, R., and Meehl, G.: An overview of CMIP5 and the experiment design, *B. Am. Meteorol. Soc.*, 93, 485–498, doi:10.1175/BAMS-D-11-00094.1, 2012.

- Thompson, D. and Wallace, J.: Regional climate impacts of the Northern Hemisphere annular mode, *Science*, 293, 85–89, doi:10.1126/science.1058958, 2001.
- Tilinina, N., Gulev, S., and Bromwich, D.: New view of Arctic cyclone activity from the Arctic system reanalysis, *Geophys. Res. Lett.*, 41, 1766–1772, doi:10.1002/2013GL058924, 2014.
- 855 Tjiputra, J., Assmann, K., Bentsen, M., Bethke, I., Otterå, O., Sturm, C., and Heinze, C.: Bergen Earth system model (BCM-C): Model description and regional climate-carbon cycle feedbacks assessment, *Geosci. Model Dev.*, 3, 123–141, doi:10.5194/gmdd-2-845-2009, 2010.
- Trenberth, K., Jones, P., Ambenje, P., Bojariu, R., Easterling, D., Klein Tank, A., Parker, D., Rahimzadeh, F., Renwick, J., Rusticucci, M., Soden, B., and Zhai, P.: Observations: Surface and atmospheric climate change. In: *Climate Change 2007: The Physical Science Basis. Contribution of Working Group I to the Fourth Assessment Report of the Intergovernmental Panel on Climate Change*, Tech. rep., Intergovernmental Panel on Climate Change (IPCC), Cambridge, United Kingdom and New York, USA, 2007.
- Ulbrich, U., Leckebusch, G., and Pinto, J.: Extra-tropical cyclones in the present and future climate: A review, *Theor. Appl. Climatol.*, 96, 117–131, doi:10.1007/s00704-008-0083-8, 2009.
- 860 van Vuuren, D., Edmonds, J., Kainuma, M., Riahi, K., Thomson, A., Hibbard, K., Hurtt, G., Kram, T., Krey, V., Lamarque, J.-F., Masui, T., Meinshausen, M., Nakicenovic, N., Smith, S., and Rose, S.: The representative concentration pathways: An overview, *Climatic Change*, 109, 5–31, doi:10.1007/s10584-011-0148-z, 2011.
- Vose, R., Applequist, S., Bourassa, M., Pryor, S., Barthelmie, R., Blanton, B., Bromirski, P., Brooks, H., DeGaetano, A., Dole, R., Easterling, D., Jensen, R., Karl, T., Katz, R., Klink, K., Kruk, M., Kunkel, K., MacCracken, M., Peterson, T., Shein, K., Thomas, B., Walsh, J., Wang, X., Wehner, M., Wuebbles, D., and Young, R.: Monitoring and understanding changes in extremes: Extratropical storms, winds, and waves, *B. Am. Meteorol. Soc.*, 95, 377–386, doi:10.1175/BAMS-D-12-00162.1, 2014.
- Walsh, J., Chapman, W., Romanovsky, V., Christensen, J., and Stendel, M.: Global climate model performance over Alaska and Greenland, *J. Climate*, 21, 6156–6174, doi:10.1175/2008JCLI2163.1, 2008.
- 870 Wang, X., Swail, V., and Zwiers, F.: Climatology and changes of extratropical cyclone activity: Comparison of ERA-40 with NCEP-NCAR reanalysis for 1958–2001, *J. Climate*, 19, 3145–3166, doi:10.1175/JCLI3781.1, 2006.
- Wang, X., Feng, Y., Compo, G., Swail, V., Zwiers, F., Allan, R., and Sardeshmukh, P.: Trends and low frequency variability of extra-tropical cyclone activity in the ensemble of twentieth century reanalysis, *Clim. Dynam.*, 40, 2775–2800, doi:10.1007/s00382-012-1450-9, 2013.
- 875 Zahn, M. and von Storch, H.: A long-term climatology of North Atlantic polar lows, *Geophys. Res. Lett.*, 35, L22 702, doi:10.1029/2008GL035769, 2008.
- Zappa, G., Shaffrey, L., and Hodges, K.: The ability of CMIP5 models to simulate North Atlantic extratropical cyclones, *J. Climate*, 26, 5379–5396, doi:10.1175/JCLI-D-12-00501.1, 2013a.
- 880 Zappa, G., Shaffrey, L., Hodges, K., Sansom, P., and Stephenson, D.: A multimodel assessment of future projections of North Atlantic and European extratropical cyclones in the CMIP5 climate models*, *J. Climate*, 26, 5846–5862, doi:10.1175/JCLI-D-12-00573.1, 2013b.
- Zappa, G., Hawcroft, M., Shaffrey, L., Black, E., and Brayshaw, D.: Extratropical cyclones and the projected decline of winter Mediterranean precipitation in the CMIP5 models, *Clim. Dynam.*, 45, 1–12, doi:10.1007/s00382-014-2426-8, 2014a.
- 885

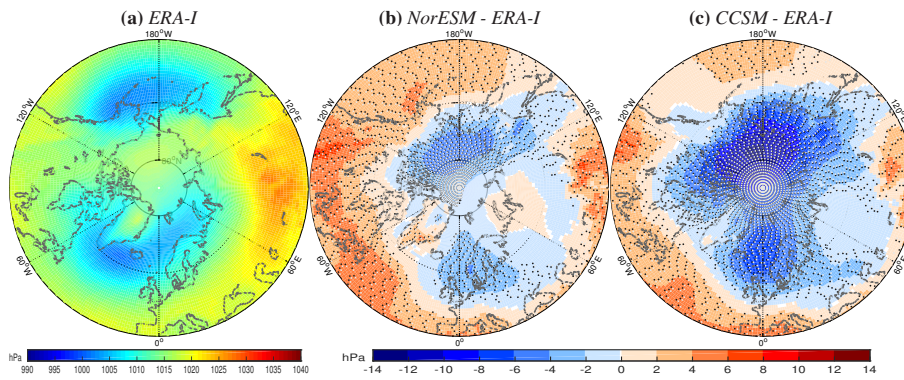


Figure 1. Sea level pressure average for SON 1979–2005 in (a) ERA-I and bias of (b) NorESM and (c) CCSM relative to ERA-I. Alternating black and white dots in (b) and (c) mark regions of significant bias at a 95 % confidence level.

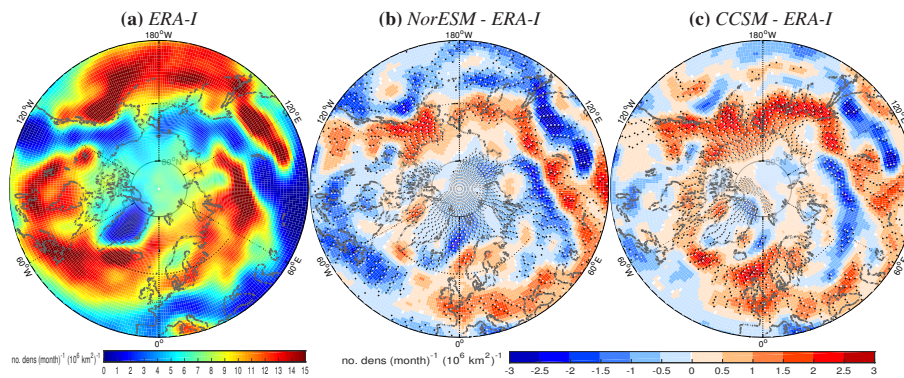


Figure 2. Track density average for SON 1979–2005 in (a) ERA-I and bias of (b) NorESM and (c) CCSM relative to ERA-I. Alternating black and white dots in (b) and (c) mark regions where $p < 0.05$ based on 2000 samples.

Zappa, G., Shaffrey, L., and Hodges, K.: Can polar lows be objectively identified and tracked in the ECMWF operational analysis and the ERA-Interim reanalysis?, *Mon. Weather Rev.*, 142, 2596–2608, doi:10.1175/MWR-D-14-00064.1, 2014b.

890 Zhang, X., Walsh, J., Zhang, J., Bhatt, U., and Ikeda, M.: Climatology and interannual variability of Arctic cyclone activity: 1948–2002, *J. Climate*, 17, 2300–2317, doi:10.1175/1520-0442(2004)017<2300:CAIVOA>2.0.CO;2, 2004.

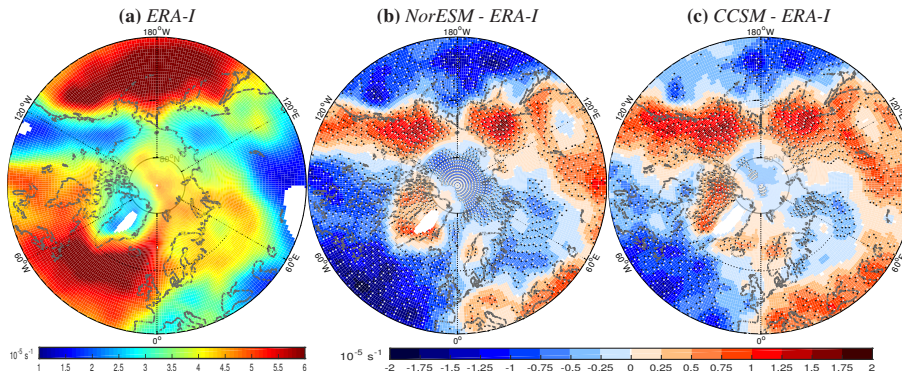


Figure 3. Mean intensity average for SOND 1979–2005 in (a) ERA-I and bias of (b) NorESM and (c) CCSM relative to ERA-I. Regions with track density below $0.5 \text{ no. density (month)}^{-1} (10^6 \text{ km}^2)^{-1}$ are shaded white. Alternating black and white dots in (b) and (c) mark regions where $p < 0.05$ based on 2000 samples.

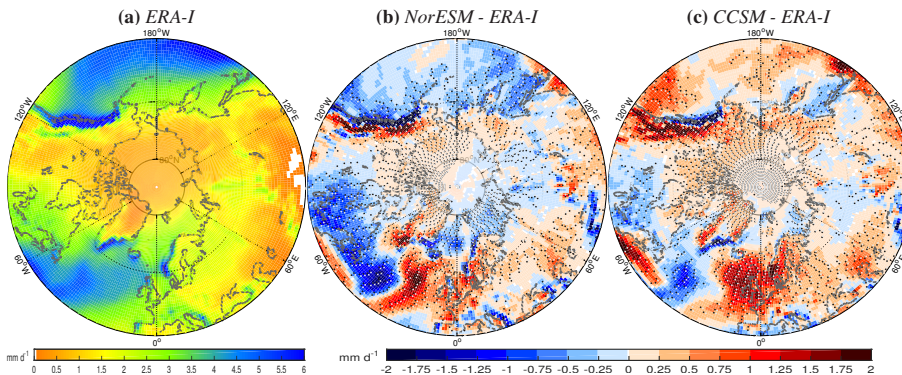


Figure 4. Precipitation average for SOND 1979–2005 in (a) ERA-I and bias of (b) NorESM and (c) CCSM relative to ERA-I. Alternating black and white dots in (b) and (c) mark regions of significant bias at a 95 % confidence level.

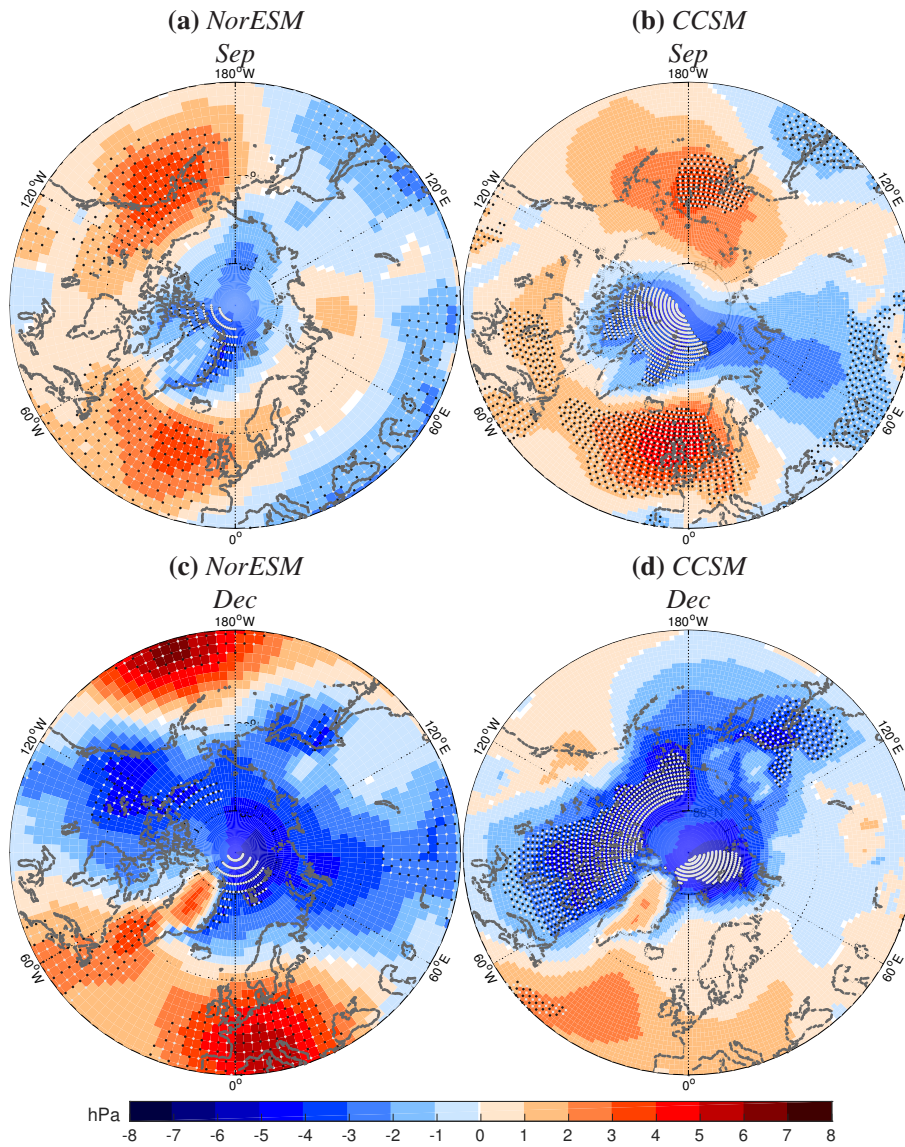


Figure 5. Changes in sea level pressure averages for September (upper row) and December (lower row) 2074–2100 relative to 1979–2005 following the RCP8.5 scenario in (a), (c) NorESM and (b), (d) CCSM. Alternating black and white dots mark regions of significant change at a 95 % confidence level.

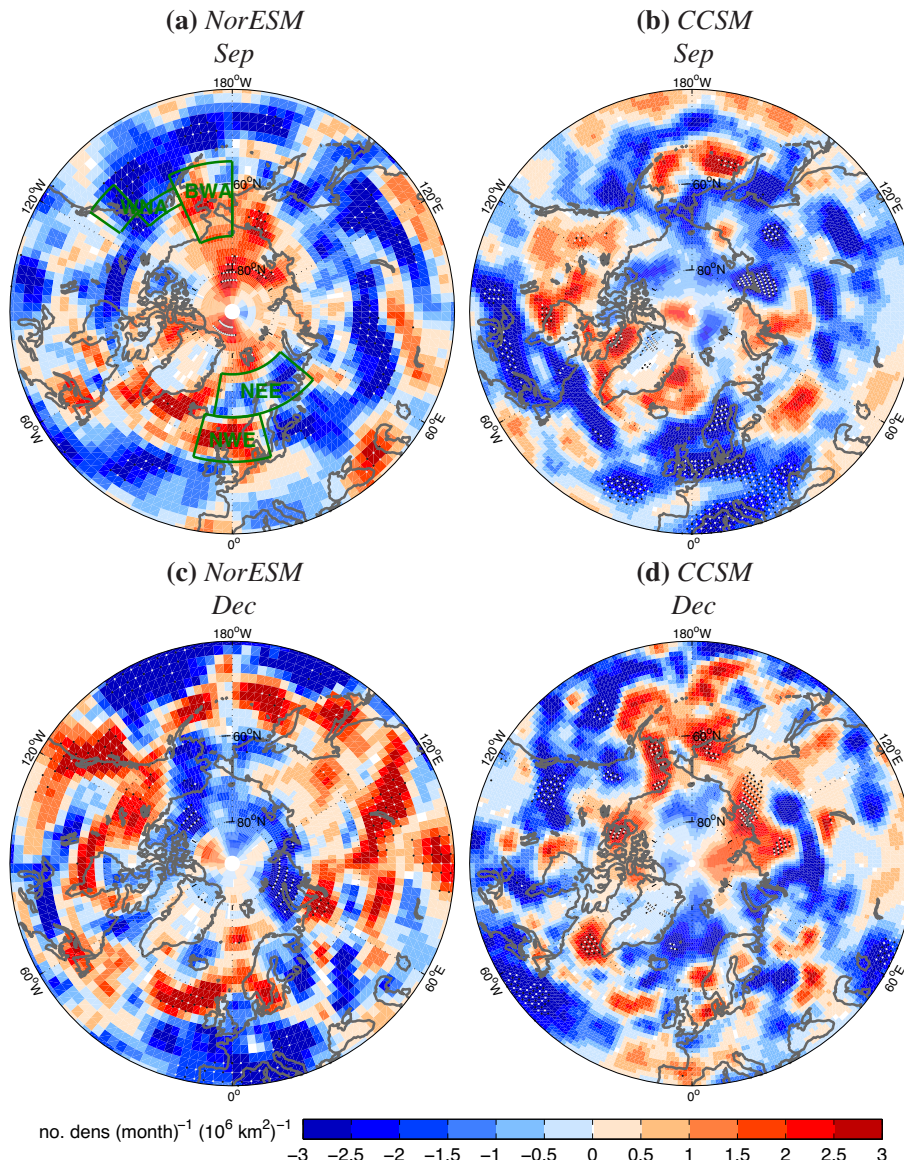


Figure 6. Changes in track density averages for September (upper row) and December (lower row) 2074–2100 relative to 1979–2005 following the RCP8.5 scenario in (a), (c) NorESM and (b), (d) CCSM. Alternating black and white dots mark regions where $p < 0.05$ based on 2000 samples. Green boxes in (a) show the four regions in Table 3.

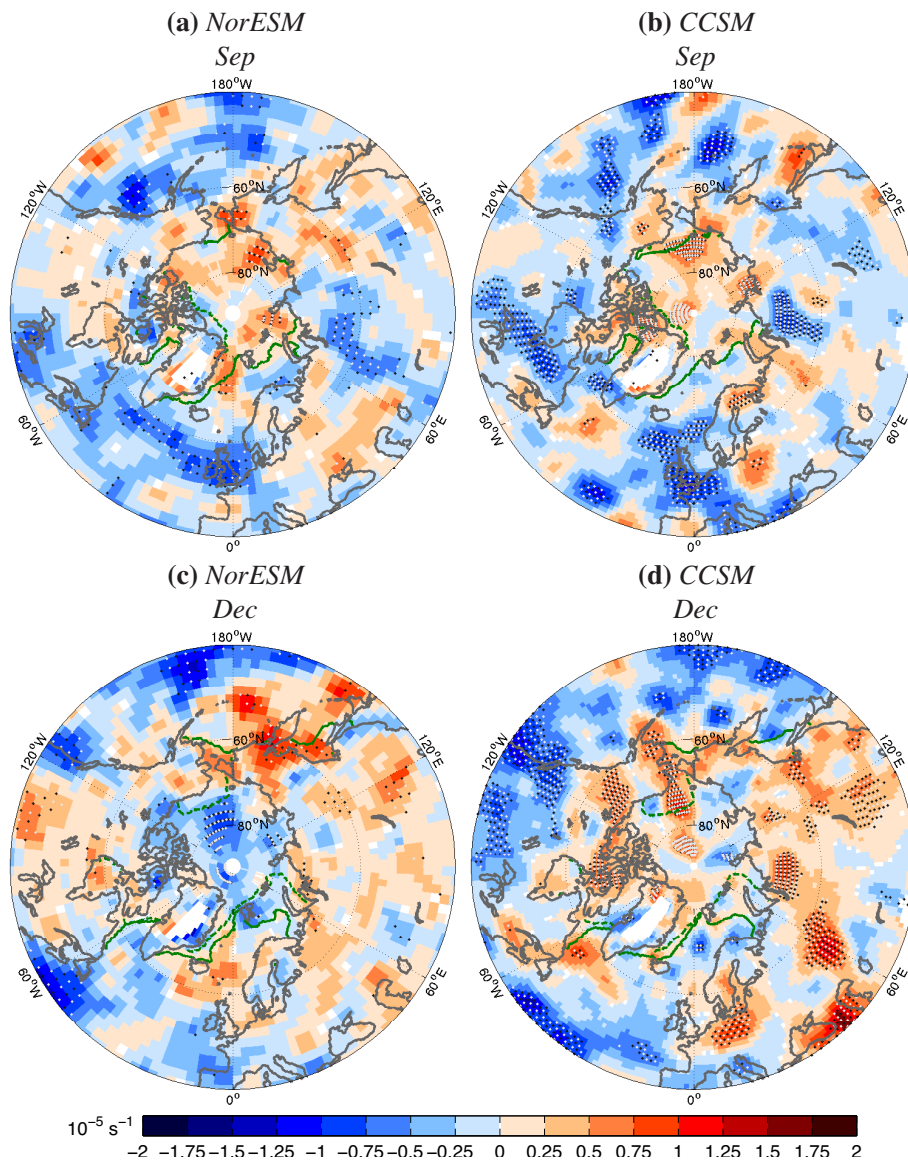


Figure 7. Changes in mean intensity averages for September (upper row) and December (lower row) 2074–2100 relative to 1979–2005 following the RCP8.5 scenario in (a), (c) NorESM and (b), (d) CCSM. Regions with track density below $0.5 \text{ no. density (month)}^{-1} (10^6 \text{ km}^2)^{-1}$ in the historical time period are shaded white. Alternating black and white dots mark regions where $p < 0.05$ based on 2000 samples. Solid and dashed green lines show the sea ice boundaries in each model and month over 1979–2005 and RCP8.5 2074–2100, respectively, calculated using a threshold of 15 % SIC.

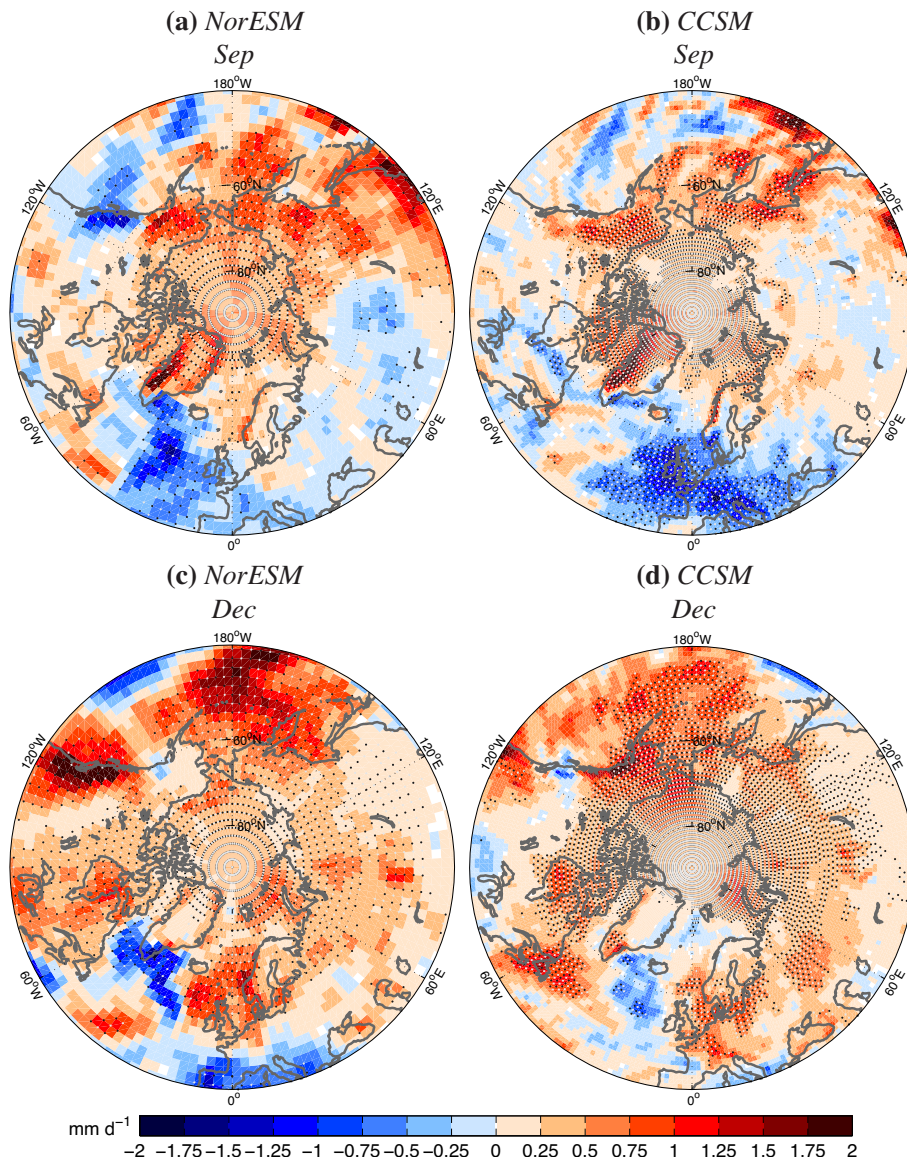


Figure 8. Changes in precipitation averages for September (upper row) and December (lower row) 2074–2100 relative to 1979–2005 following the RCP8.5 scenario in (a), (c) NorESM and (b), (d) CCSM. Alternating black and white dots mark regions of significant change at a 95 % confidence level.

Table 1. Decadal mean Arctic sea ice extent monthly averages for 2000's, 2050's and 2090's and changes for the two latter decades compared to the former, following the RCP8.5 scenario. 2000's: First number within row from NSIDC; second number within row from NorESM; third number within row from CCSM. Other decades: First number within each row from NorESM; second number within each row from CCSM. Unit is 10^6 km^2 .

Decade	Jan	Feb	Mar	Apr	May	Jun	Jul	Aug	Sep	Oct	Nov	Dec
2000's	14.1	14.9	15.1	14.3	13.1	11.5	9.1	6.5	5.7	8.3	10.4	12.6
	13.1	14.0	14.7	14.2	13.3	11.7	10.2	9.0	7.8	9.2	10.6	12.1
2050's	12.4	13.0	13.2	12.8	11.9	10.4	8.7	6.6	5.5	7.3	8.8	10.8
	10.7	11.9	12.7	12.5	11.5	9.9	8.3	6.9	5.5	6.0	7.1	8.9
2090's	10.0	10.8	11.2	10.8	10.3	9.1	5.3	0.8	0.8	1.1	4.4	7.8
	8.8	10.1	11.1	11.0	9.7	7.6	4.8	2.3	0.3	1.4	3.7	6.2
$\Delta 2050$'s	6.6	9.1	9.9	9.8	9.3	7.2	1.7	0	0	0	0.3	2.8
	-2.4	-2.1	-2.0	-1.7	-1.8	-1.8	-1.9	-2.1	-2.3	-3.2	-3.5	-3.2
$\Delta 2090$'s	-2.4	-2.2	-2.0	-2.0	-1.6	-1.3	-3.4	-5.8	-4.7	-6.2	-4.4	-3.0
	-4.3	-3.9	-3.6	-3.2	-3.6	-4.1	-5.4	-6.7	-7.5	-7.8	-6.9	-5.9
	-5.8	-3.9	-3.3	-3.0	-2.6	-3.2	-7.0	-6.6	-5.5	-7.3	-8.5	-8.0

Table 2. Time period mean sea level pressure (SLP), track density (tden), mean intensity (mint) and precipitation (P) SOND averages for 1979–2005 (1979–2005) and changes for 2074–2100 relative to 1979–2005 following the RCP8.5 scenario ($\Delta 2074$ –2100) in ERA-I, NorESM and CCSM. First number within each column denotes average over midlatitudes (40 – 65°N); second number within each column denotes average over high-latitudes (65 – 90°N). For 1979–2005, units are hPa, $\text{no. dens (month)}^{-1}$ (10^6 km^2) $^{-1}$, 10^{-5} s^{-1} and mm d^{-1} for SLP, tden, mint and P, respectively. For $\Delta 2074$ –2100, unit is %.

Data set	Time period	SLP		tden		mint		P	
ERA-I	1979–2005	1015	1012	9.0	7.0	4.2	3.7	2.5	1.2
NorESM	1979–2005	1016	1010	8.9	6.8	4.0	3.8	2.5	1.2
	$\Delta 2074$ –2100	0.02	-0.24	-3.9	0.3	-0.2	0.9	10.7	38.2
CCSM	1979–2005	1015	1006	9.5	7.7	4.2	3.9	2.8	1.4
	$\Delta 2074$ –2100	0.02	-0.18	-6.5	-0.8	-1.7	2.9	8.0	31.8

Table 3. Changes of track density (tden; first row), mean intensity (mint; second row) and precipitation (P; third row) over September and December for 2074–2100 relative to 1979–2005 following the RCP8.5 scenario in NorESM and CCSM in four North Atlantic and North Pacific storm track regions. The regions are western North America (WNA; 50–58°N, 125–137°W and 58–62°N, 136–155°W), Bering and western Alaska (BWA; 55–72°N, 155–180°W), northwestern Europe (NWE; 55–65°N, 15°W–15°E) and northeastern Europe (NEE; 65–75°N, 10°W–50°E). First number within each column denotes change in September; second number within each column denotes change in December. Unit is %.

Parameter	Data set	WNA		BWA		NWE		NEE	
tden	NorESM	-20.1	18.2	11.3	-13.4	12.8	10.2	-6.5	-0.8
	CCSM	-8.0	-12.8	-8.1	15.5	-21.7	1.2	-1.2	-11.6
mint	NorESM	-6.2	0	-1.4	3.2	-5.9	4.2	-0.1	1.5
	CCSM	-5.2	-0.5	2.0	8.3	-8.9	1.3	0.9	-3.6
P	NorESM	-4.1	15.5	23.8	21.5	5.7	19.7	11.7	21.1
	CCSM	5.8	10.1	18.0	44.4	-12.0	8.7	13.0	5.3